Deep Resources Engineering 1 (2024) 100007

Contents lists available at ScienceDirect

Deep Resources Engineering

journal homepage: www.keaipublishing.com/en/journals/deepre/

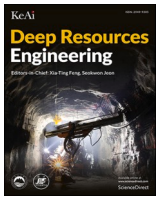

Full Length Article

Rock engineering evaluation of existing and planned Salang Tunnels with high overburden through Hindukush Mountains, Afghanistan

N. Malistani *, Ö. Aydan

University of the Ryukyus, Okinawa, Japan

ARTICLE INFO

Keywords:
Salang Tunnels
Stability
Rock Mass Classification Systems
Numerical Analyses
Seismicity
Squeezing
Ground Support

ABSTRACT

The Kabul – Mazar Highway connects Kabul, the capital of Afghanistan, to northern provinces of the country, and further extends into Central Asian countries through the Hindukush mountains. The Salang Tunnel, which is 2600 m long, was designed by Soviet engineers in 1958 and constructed using conventional techniques in 1964. During its construction, the tunnel ranked the distinction of being the highest-altitude tunnel at 3400 m. The socioeconomic importance of the tunnel is exceptionally high, as the Hindukush Mountain range to the east and south of the country is crossed by it. Since 1964, there has been a significant increase in traffic volume. Due to the narrowness of the existing tunnel, the Ministry of Public Works (MOPW) of Afghanistan has planned the construction of new twin-tube tunnels. Although there have been rehabilitation and enlargement efforts for the existing tunnel, none of these renovation works have been proven effective, and challenges persist. In 2008, the MOPW initiated a pre-feasibility study for new tunnels, which was finalized in 2012, presenting various options. Subsequently, in early 2018, the MOPW commenced feasibility and detailed studies, leading to the proposal of new twin-tube tunnels, which are designated as the planned tunnels in this paper. In this study, the available geotechnical and environmental data are used to evaluate the rock engineering aspects of the tunnels, including an assessment of the in-situ stress state. A particular emphasis is placed on the reassessment and design of the support system for both the existing and planned tunnels according to RMQR and another system, respectively. The evaluation of the response and stability of the tunnels is concluded, and the implications are subsequently discussed.

1. Introduction

The existing Salang Tunnel is a 2.6-kilometer-long tunnel situated at the Salang Pass in the Hindukush Mountains, connecting the Parwan and Baghlan provinces of Afghanistan. It is located at the chainage of 113.9 km on the Kabul-Mazar highway (AH-76). The tunnel serves as a crucial link for Afghanistan, facilitating access to the countries of Central Asia and Russia (Figs. 1 and 2). The alignment of the existing tunnel is oriented in a north- northeast/south-southeast direction, with approximate coordinates of E69.06225° and N35.29765°. The tunnel has dimensions of approximately 8.40 m in width and 7 m in height, featuring a horseshoe-shaped cross-section. It was constructed in the 1960 s, and its north and south portals are situated at elevations of 3400 m and 3360 m, respectively. The tunnel was the highest altitude tunnel at the time of construction. Unfortunately, the tunnel experienced explosions during the civil war, leading to its closure to traffic in the 1990 s due to a significant blast that resulted in substantial tunnel damage.

The tunnel entrances and the nearby mountains experience challenging environmental conditions, including cycles of freezing and thawing. The tunnel was designed for 1000 vehicles per day. Since 1964, there has been a significant increase in traffic volume. Due to the narrowness of the existing tunnel, the Ministry of Public Works (MOPW) of Afghanistan has planned the construction of new twin-tube tunnels. Although there have been rehabilitation and enlargement efforts for the existing tunnel, none of these renovation works have been proven effective, and challenges persist. However, approximately 16,000 vehicles passed the Salang Tunnel daily in 2010 [42,41]. The Hindukush Mountains are the prominent geographical feature in Northen Afghanistan, stretching in a northeast-southwest direction and covering over 49 percent of the entire land, with peaks reaching elevations as high as 7708 m above sea level.

The government decided to start a pre-feasibility study of new tunnels in 2008 and completed it in 2012 with the proposal of several options. Later, feasibility and detailed studies started in early 2018 and

* Corresponding Author.
E-mail address: neamat67@gmail.com (N. Malistani).

https://doi.org/10.1016/j.deepre.2024.100007
Received 2 October 2023; Received in revised form 5 March 2024; Accepted 6 March 2024
Available online 22 March 2024

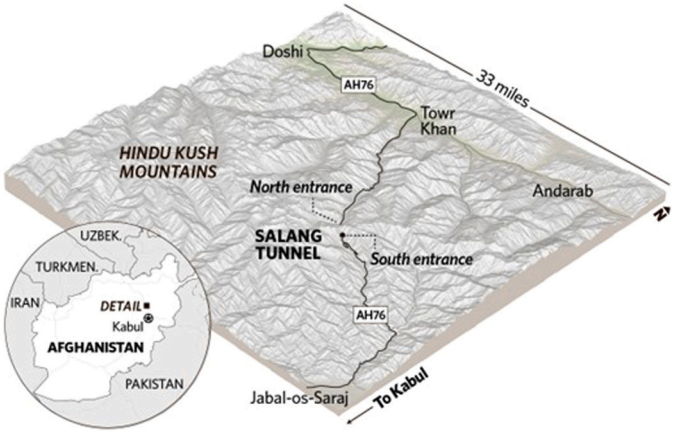

Fig. 1. Location of the Salang Tunnel (from [42,40]).

proposed new twin-tube tunnels which are designated as the planned new tunnels in this study. The new twin-tube tunnels, situated approximately 500 m to the east of the existing Salang Tunnel, have a length of roughly 6800 m, with a pillar width of approximately 25 meters between them. Each tunnel has 9.5 m width and 6.42 m height at an elevation of 3060 m in south portal and 3200 at north portal. The geological conditions of the planned tunnels are expected to be similar to the existing tunnel. However, the planned tunnels have a significantly greater overburden, approximately 900 m, which is approximately 500 m higher than that of the existing tunnel.

This paper utilizes existing geotechnical data along with newly acquired geotechnical and environmental data to conduct a rock engineering assessment of both the existing and planned Salang Tunnels. Some rock mechanistic laboratory tests such as uniaxial compression, triaxial and Brazilian tests have been implemented on rock samples obtained from boreholes and block samples. Some shear, stick-slip, and tilting tests are performed on the rock discontinuities. Based on borehole logs, discontinuity surveying together with physical observations the state of rock mass is evaluated using Rock Mass Quality Rating (RMQR) rock mass classification system. The in-situ stress state of the tunnel sites is estimated through various stress inference techniques. For stability assessments, rock mass properties are evaluated. The deformation response and the stability of the tunnels are assessed using kinematic analysis technique, analytical ground-reaction methods, and elasto-plastic Finite Element Method (FEM). A brief discussion on the design methodology of the tunnel support systems is presented. Then, the support systems of the existing and planned tunnels according to RMQR are presented and compared with those from the other rock mass classifications.

2. Geology

The areas surrounding both the south and north portals of the Salang Tunnel are characterized by topography that varies from gentle to steep slopes, with angles ranging from 5° to 35° at the south portal and from ranging 5° to 25° at the north portal [42,40,41]. At the southern portal, three stream channels are present, while the northern portal features five stream channels. A small amount of water flows consistently from the top, forming a small lake located above the northern portal. These streams converge downstream. The existing Salang Tunnel area primarily consists of a single rock type, which is visible in outcrops at both the southern and northern portals (Fig. 2). This rock is classified as granitic/granodiorite/plagio-granitic and dates back to the early to late Triassic period. The third rock unit comprises coarse-grained quartz, feldspar, and mica (mainly biotite) crystals, with mafic enclaves of country rock (Fig. 3). When observed at a local scale, the outcrop resembles a massive plutonic body but exhibits significant tectonic disturbances on a regional scale.

To the north of the planned tunnels, the predominant geological feature is mica schist, with localized occurrences of gneiss. There is also a 200–500-meter section characterized by heavily fractured rocks (Fig. 4). Granite forms the geological conditions for the roadway between the two tunnels. The geological contact between the granite and the metamorphic gneissic unit is faulted, and it is likely that a strike-slip fault is situated approximately in the center of the tunnel. This fault runs in an approximate east-west direction and exhibits signs of left-lateral

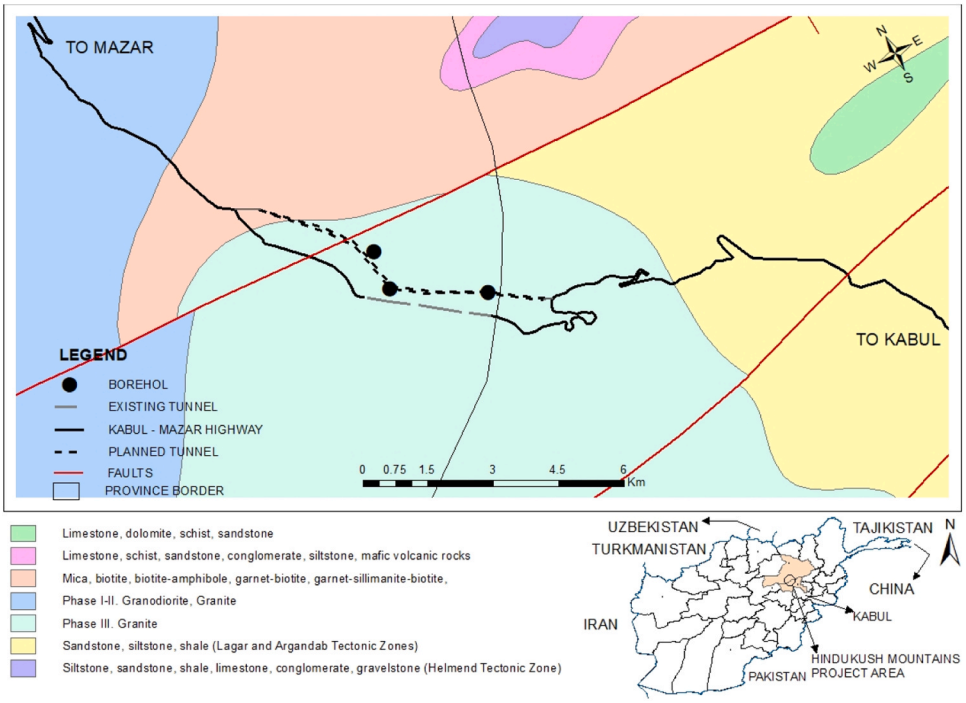

Fig. 2. Geological map and the locations of tunnels in Salang Pass.

Fig. 3. The weathered surface of granite shows thin layers of compositional banding at the northern portal. Dark bands rich in mica.

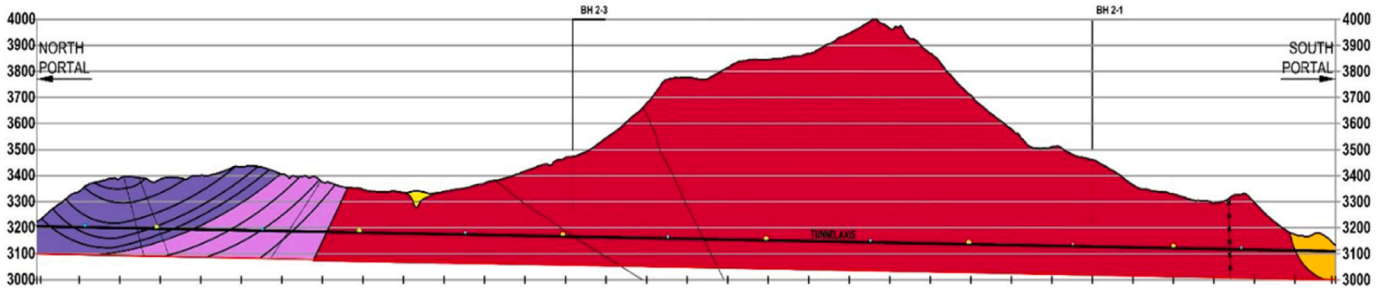

(a). Northbound Tunnel (Tube1)

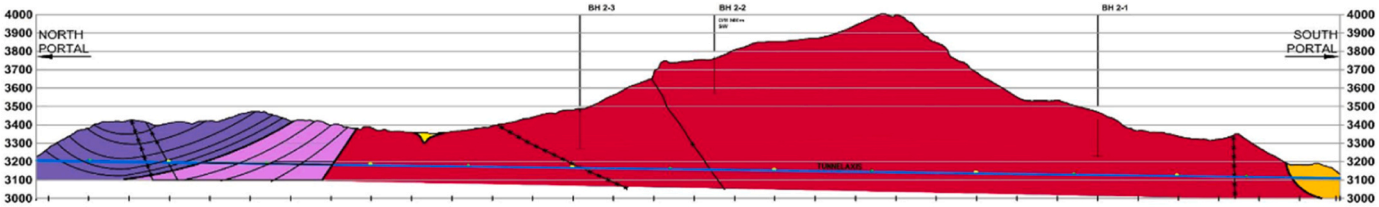

(b). Southbound Tunnel (Tube2)

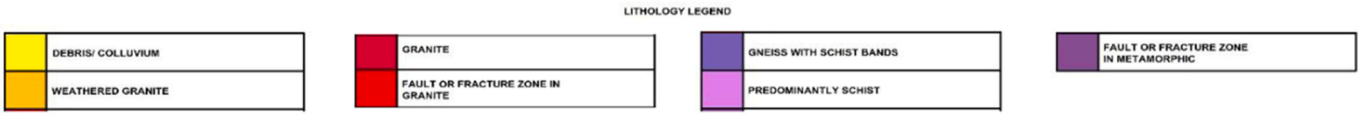

(c). Legend

Fig. 4. Geological conditions and overburden of newly planned tunnels.

movement. Moreover, the fault demarcates the boundary between the sandstone siltstone unit and the Paleoproterozoic gneiss.

3. Seismo-tectonics and maximum ground motions

The Hindukush region in Afghanistan is known for its high seismic activity, as illustrated in Fig. 5 [27,42,40]. Within this region lies the Salang Tunnel, situated within a plutonic rock mass that is bounded by two major faults. The Andarab fault acts as the northern boundary for the plutonic block and exhibits dextral faulting characteristics. This fault has an overall length of approximately 150–160 km and is believed to be segmented, with the largest segment estimated to be around 85 km in length. According to calculations based on Aydan's [15] proposed relations, this segment has the potential to generate an earthquake with a moment magnitude of 7.4 and a slip of 255 cm.

The Hari-Rod fault, also referred to as the Herat Fault, lies to the south of the Salang Tunnel and serves as the southern boundary of the plutonic body. This fault exhibits a dextral faulting pattern and converges with the sinistral Chaman fault near Jabal Saraj. It spans a total length of over 800 kilometers; however, it's important to note that this fault is divided into segments. The segment near the Salang Tunnel is approximately 64 kilometers long. The estimated moment magnitude for this segment is approximately 7.0, accompanied by a displacement of 180 cm.

Fig. 6 displays the contours of maximum ground surface accelerations for rocky terrain. These contours assume an earthquake occurring along the Andarab fault, with a rupture length of 85 km and a moment magnitude of 7.4. According to the relationships presented by Aydan [15], it is anticipated that the maximum ground acceleration at the Salang Tunnel will fall within the range of 330–390 gals. Nonetheless, in the event of an earthquake along the Hari-Rod fault, characterized by a rupture length of 64 km, the maximum ground acceleration is projected to span between 220 and 260 gals. Therefore, the earthquake on the Andarab Fault is much more critical for the Salang Tunnel.

4. Laboratory and index tests

4.1. Laboratory tests

The laboratory experiments were carried out by the authors on samples extracted from a large block near the south portal of the existing Salang Tunnel. Some point-load tests, uniaxial compression, Brazilian and triaxial tests were carried out by the Ministry of Public Works (MOPW) in relation to the rehabilitation of the existing tunnel and planned tunnels. The most of laboratory tests reported in this section were conducted by the authors in the Rock Mechanics Laboratory of the University of the Ryukyus (UR).

4.1.1. Index tests

Point-load tests were carried out on outcrops and borehole samples, which were obtained from the existing tunnel and newly planned tunnel alignment. The values of point-load tests are quite variable, and they range between 1.26 and 5.42. The average values of the UCS inferred point-load tests ranged between 27.71 and 119.25 MPa.

A series of index tests such as P-wave and S-wave velocities, equotip rebound number (LEEB), unit weights were conducted on the samples. Table 1 summarizes the results of some of index tests. As noted from the table, the index properties decrease as the state of intact rock changes from "fresh" to "weathered".

4.1.2. Uniaxial compression tests

A series of uniaxial compression experiments were conducted. During tests acoustic emissions and acceleration were measured besides the measurements of strain and stress. One example of uniaxial compression experiments is shown in Fig. 7. These experiments are expected to provide some fundamental monitoring parameters during the excavation of planned tunnels against rock burst problems, particularly. In Fig. 7, fundamental monitoring parameters such as Acoustic Emission (AE), acoustic emission rate and acceleration besides conventional strain and stress are shown, which could be useful during the excavation

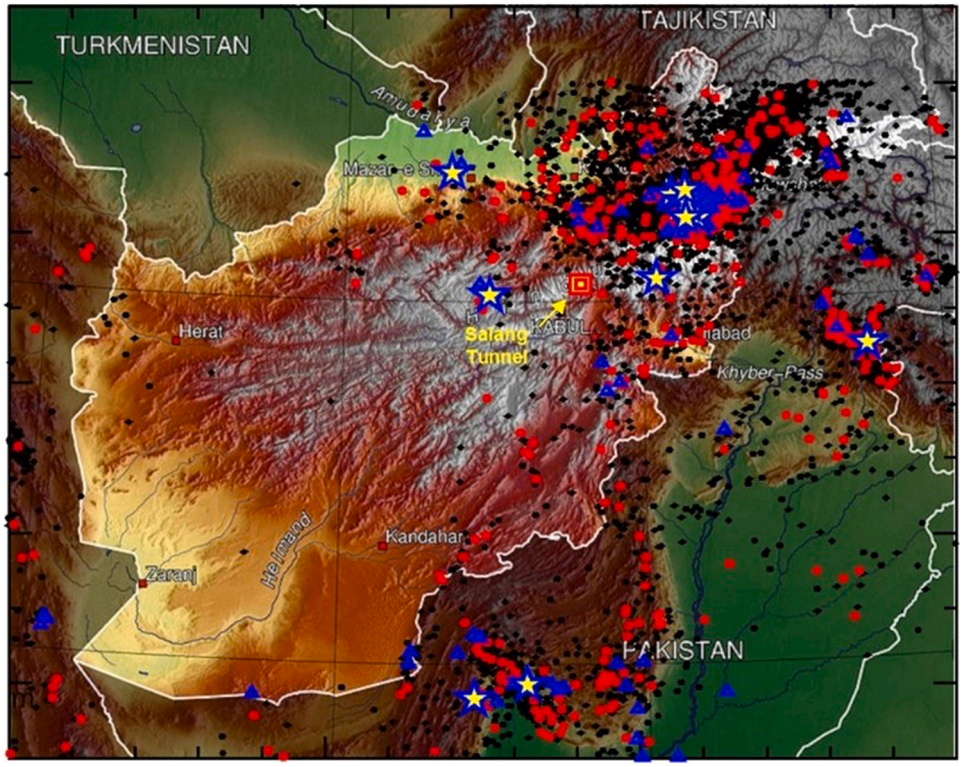

Fig. 5. The seismicity of Afghanistan [48].

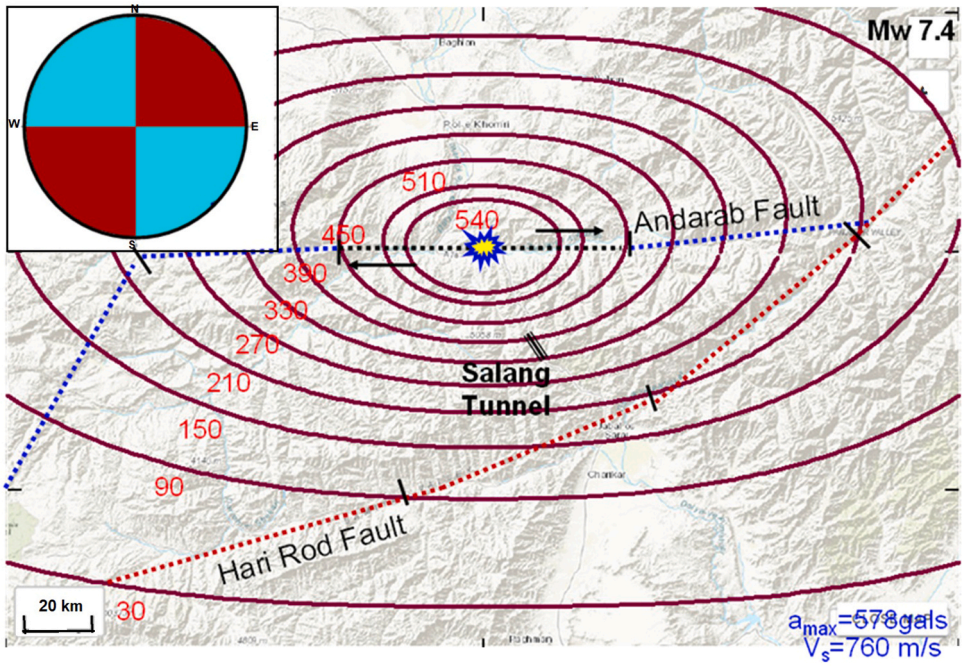

Fig. 6. Estimated maximum ground accelerations.

Table 1
A summary of index test results.

State	Unit weight	P-wave velocity (km/s)	S-wave velocity (km/s)	Equotip rebound number
Fresh	25.5–26.7	3.8–5.3	2.1–2.7	810–890
Weathered	24.4–25.2	1.3–2.0	0.65–1.2	505–645

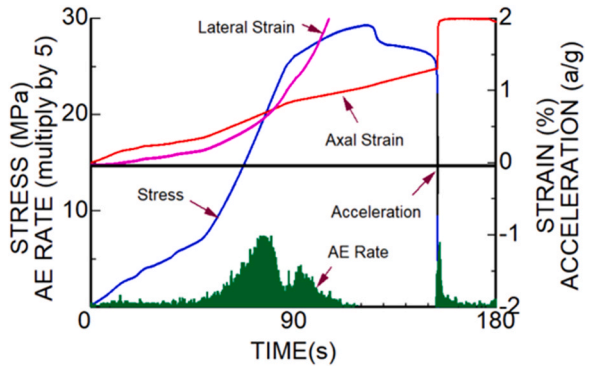

Fig. 7. Multi-parameter response of granite sample (SU3) during compression test.

of planned tunnels against rock burst problems.

4.1.3. Brazilian Tensile Strength Tests

Numerous Brazilian Tensile Strength Tests were performed on rock disks, as depicted in Fig. 8, which illustrates the testing process and provides a post-test view of the samples. The experimental findings closely align with those reported by the Ministry of Public Works. In our tests, the Brazilian tensile strength varied from 1.6 to 2.2 MPa (Fig. 9).

4.1.4. Triaxial tests

Ministry of Public Works of Afghanistan reported some triaxial tests carried out under a confining pressure of 5, 10, 15 and 20 MPa. While

Fig. 8. Views of a Brazilian test and a tested sample.

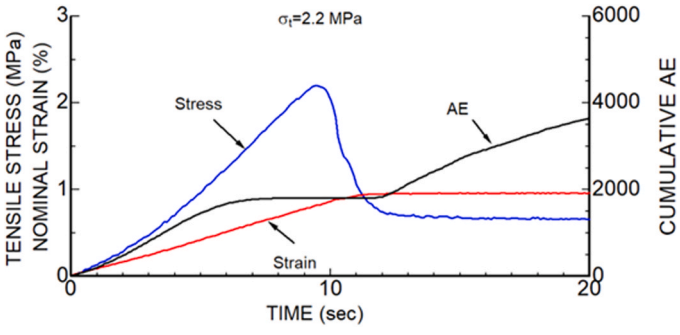

Fig. 9. Measured responses during a Brazilian tensile strength test.

they attempted to infer the uniaxial compressive strength from yield functions fitted to the yield criteria. Actually, such evaluations should have had to include the tensile and compressive strength, in addition to triaxial testing data from the same sample lot. The inferred uniaxial

compressive strength was extremely low down to 12.3 MPa. Furthermore, the results were highly scattered,

4.1.5. Yield criteria

Although there are many yield criteria (e.g., [11,21]), Mohr-Coulomb yield criterion was selected as the most common one and the parameters were determined from tensile strength and uniaxial compressive strength. Figs. 10 and 11 show the fitted yield criteria for the data reported by the MOPW and this study. The cohesion and friction angle for each situation are indicated in the figures. The MOPW classifies intact rock as fresh (Peak), slightly weathered (mean) and moderately weathered (lower). The friction angle of the intact rock is estimated to be greater than 60 degrees. The yield criterion fitted to our experimental data yielded the friction angle to be almost the same as those reported by the MOPW. On the other hand, our experimental values for cohesion are close to that of moderately weathered granite according to the classification of the MOPW. In view of the sampling location, the rock block sample was likely to be moderately weathered.

4.1.6. Tilting and stick-slip tests

Tilting tests to determine the friction angle of saw-cut planes and natural discontinuities at the existing tunnel site were conducted under both dry and immersed conditions [28]. The results are summarized in Table 2. The tilting tests on natural discontinuities were carried out parallel and perpendicular to ridges (Fig. 12). The friction angle of natural discontinuities was generally greater than 40 degrees.

The stick-slip tests results on the discontinuities of Salang granite were carried out and the results are reported in a recent publication by Aydan et al. [28]. The frictional properties (static and kinetic) obtained from stick-slip tests are also compared with those from tilting tests as given in Table 3. The results are quite similar to each other despite different testing techniques are used. The kinetic friction property is particularly important to evaluate post-failure motions of failing bodies.

4.1.7. Dynamic shear testing of discontinuities

Dynamic shear experiments of Salang granite were conducted under three different normal stress levels (Fig. 13). Fig. 14 shows the locus of dynamic shear behavior in the space of displacement and friction coefficient under a normal load level of approximately 10 N [9]. The peak friction angle was about 42 degrees while the kinetic friction angle was reduced to about 26 degrees. Particularly the peak friction angle is close to that from tilting and stick-slip tests.

4.2. Multi-parameter response of a circular model tunnel in Salang granite block

As the overburden of the planned Salang Tunnels is quite high, rock burst might be a great issue in actual excavations. To have some insight view of the response of a circular opening, a granite block sample was gathered from the existing Salang Tunnel site and some laboratory experiments were carried out. The diameter of the circular opening drilled

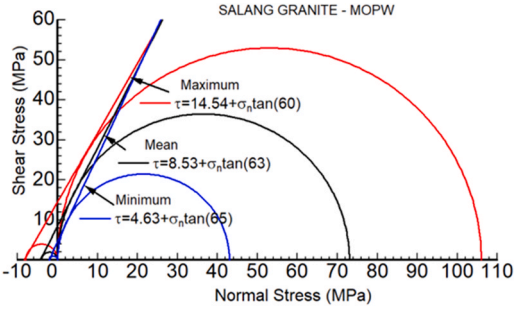

Fig. 10. Mohr-Coulomb yield envelopes for the experimental results reported by MOPW [43].

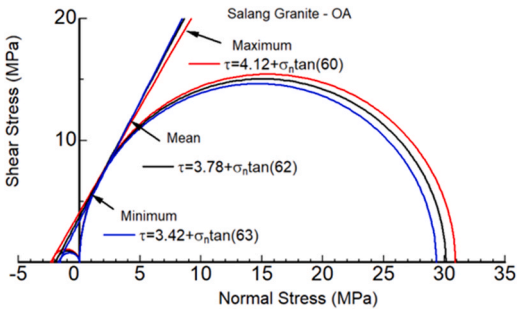

Fig. 11. Mohr-Coulomb yield envelopes for our experimental results.

Table 2
Frictional angles of saw-cut planes and natural discontinuities; Salang Tunnel.

Planes		Dry (ϕ)	Immersed (ϕ)
Saw-cut planes	50 ×75 mm	34–36	32–34
	150 ×150 mm	35–37	33–34
Natural discontinuities	parallel to ridges and grooves	40–43	40–44
	perpendicular to ridges and grooves	41–45	45–46

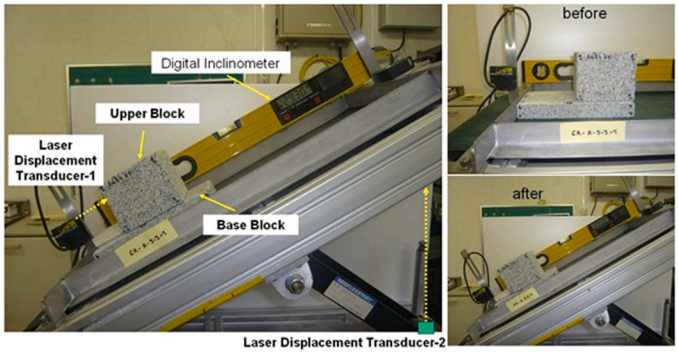

Fig. 12. Views of a typical tilting test [28].

Table 3
Comparison of average static and kinetic friction angles (from tilting and stick-slip tests).

Tilting		Stick-slip	
Static (ϕ)	Kinetic (ϕ)	Static (ϕ)	Kinetic (ϕ)
43.2	37.2	41.6	35.8

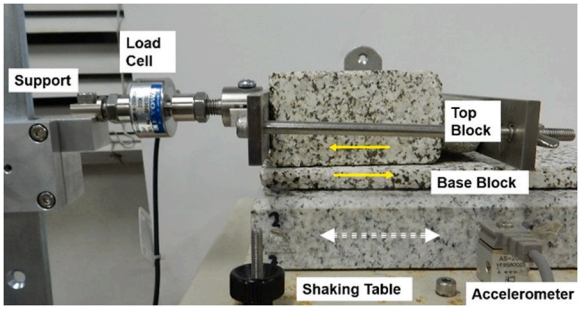

Fig. 13. Dynamic shear test set-up a post-test view of discontinuity.

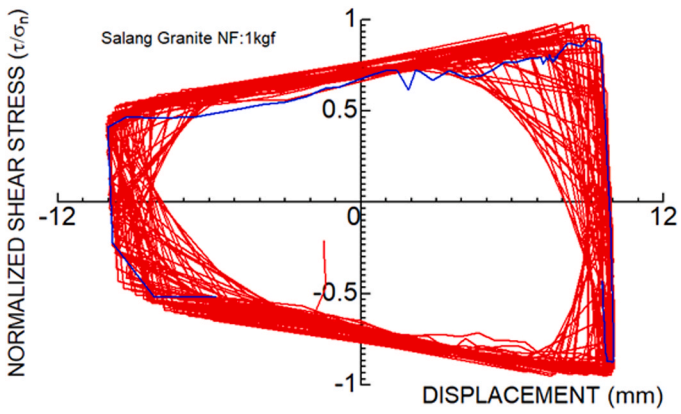

Fig. 14. Dynamic shear behavior of discontinuities of Salang granite.

into the granite sample was 50 mm. The specimen was instrumented with strain gauges, acoustic emissions sensors and accelerometers besides applied load and global displacement responses. Furthermore, infrared thermography imaging was carried out during this test (Fig. 15). The testing procedures described were similar to the previous studies [7,17,10,23].

Fig. 16 indicates some of the responses recorded during the experiment. The presented data contains both local and global strains, applied stress, as well as acoustic emissions at the roof and sidewalls. As it can be observed from the figure, several remarkable observations can be made. At the end of the experiment, permanent strains in the sidewalls, roof and total strain were observed. Additionally, the Kaiser effect was distinctly observed during the initial loading-unloading cycle. It's important to note that the sample did not experience complete failure.

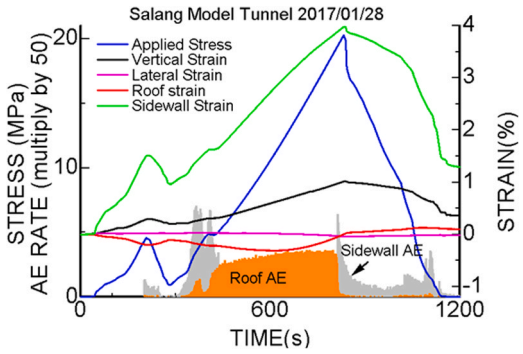

Fig. 16. Multi-parameter reactions of the model tunnel in a large rock sample.

An elasto-plastic finite element analysis of the model test was conducted, and certain results are represented in Fig. 17. Although the model itself was not loaded up to failure, this type analyses provide some insight view of stress concentration and the possible fracturing pattern.

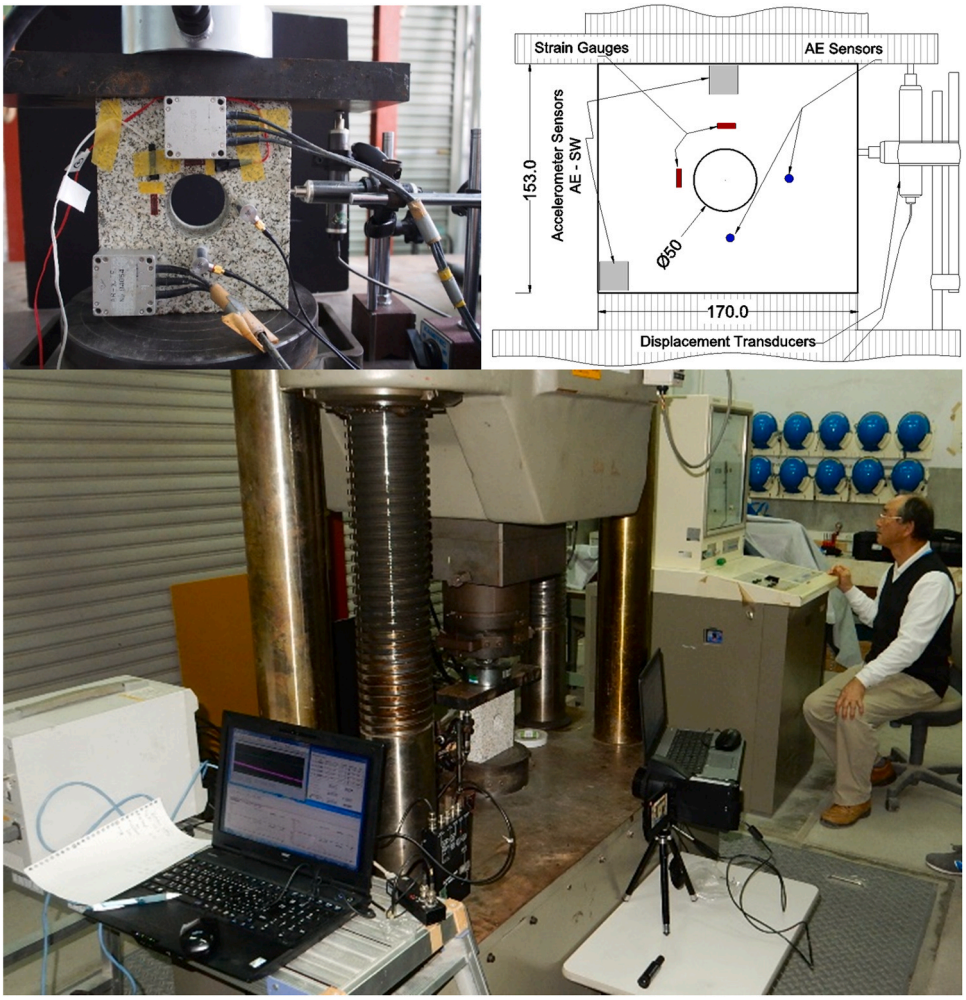

Fig. 15. A general view of the test and the back-side of the instrumented sample.

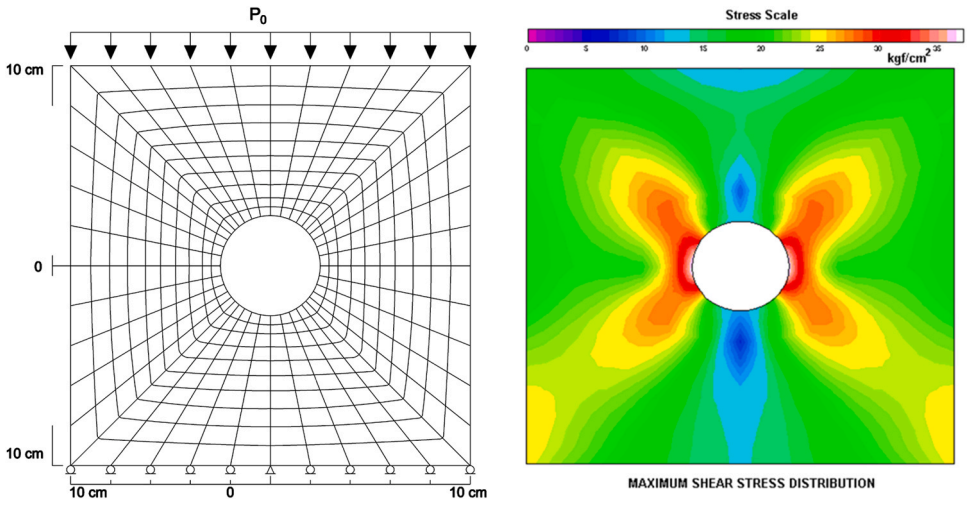

Fig. 17. Finite element mesh and the distribution of maximum shear stress in the model block.

5. Characterization of rock mass

5.1. The existing Salang Tunnel

Rock masses observed at outcrops exhibit significant weathering, jointing, and fracturing. Detailed examinations of outcrops at both the south and north portals of the tunnel were conducted, and orientations of the discontinuities were measured along specific scanlines. Fig. 18 illustrates a stereo-projection of the major discontinuities. Site investigations revealed the presence of four significant discontinuity sets [42,40].

The characterization of rock masses at the north and south portals was conducted using the RMQR rock classification system. The outcomes are presented in Tables 4 and 5 for the south and north portals, respectively. Notably, there are several critical discontinuities sets whose strike nearly parallels the tunnel axis.

5.2. The newly planned Salang Tunnels

As the newly planned tunnels are about 200 m below the existing

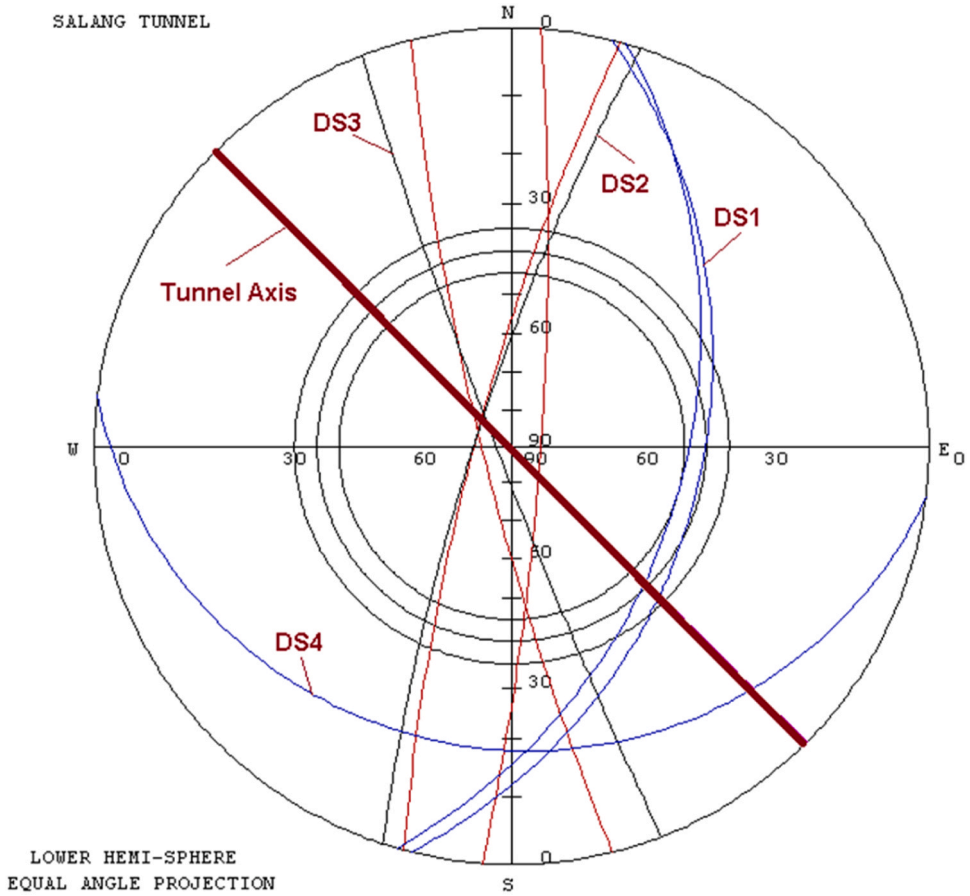

Fig. 18. The south and north portals stereo-projection of discontinuity.

Table 4
RMQR rates for the south portal.

Parameters	Description	Rating
R_{DD}	Heavy/moderate degradation	3–6
R_{DSN}	Three set plus random	8
R_{DS}	1.2 m>DS>0.3 m	8
R_{DC}	Smooth/tight to rough	15–22
R_{GWSC}	Wet to dripping	3–5
R_{GWAC}	Slightly absorptive	4
	RMQR	41–62

Table 5
RMQR rates for the north portal.

Parameters	Description	Rating
R_{DD}	Moderate/slight degradation	6–9
R_{DSN}	Three set plus random	8
R_{DS}	1.2 m>DS>0.3 m	8
R_{DC}	Smooth/tight to rough	15–22
R_{GWSC}	Wet to dripping	3–5
R_{GWAC}	Slightly absorptive	4
	RMQR	44–65

tunnel and located in similar rocks, the discontinuities sets are found to be quite similar to those shown in Fig. 18. Most of observations regarding the planned tunnel were conducted at the outcrops near the portal sites and along the tunnel alignment. Additionally, five new borings, reaching a depth of 200 m from the ground surface, were carried out.

None of the borings passed through a shear zone. Rock mass is granite and gneissic schist were observed in the north portals of the planned tunnels. The weathering zone are expected to reach to certain depth, which seems to be 30–50 m into rock mass from the ground surface. In other words, the weathered zones are likely to be limited to the portal zones. Hence, the evaluations of rock mass conditions are given for fresh, weathered and fracture/shear zones and the evaluation results obtained using the RMQR Rock Mass Classifications are given in Tables 6–8. The evaluations for the fracture/shear zones fundamentally correspond to gouge or highly fractured zone. As several fracture/shear zones cross the tunnels at several locations, detailed site investigations are necessary for such zones for the possibility of squeezing behavior of tunnels during excavation in addition to rock burst possibility. Under the most extreme condition of squeezing/rockburst, the pillar will have a 15 m thick elastic core between the two tunnels. However, if the bolt length is more than 6 m together with appropriate support system consisting of shotcrete with wire mesh and steel ribs should be sufficient to control the deformation. Nevertheless, the trimming of deformed tunnels may be additional counter measures to deal with very large deformations.

6. In-situ stress evaluation

The stress state of Afghanistan is almost unknown and there is no report on in-situ measurements in Afghanistan yet except the study by Aydan et al. [27]. Nevertheless, constructing underground openings such as tunnels and underground caverns definitely require information on the stress state for stability assessments.

Table 6
The RMQR value for the fresh granite and gneissic schist.

Parameters	Description	Rating
R_{DD}	Fresh-stained	12–15
R_{DSN}	Two set plus random	12
R_{DS}	1.2 m>DS>0.3 m	8
R_{DC}	tight to rough	22
R_{GWSC}	Dry to Damp	7–9
R_{GWAC}	Non-absorptive, Capillarity	5–6
	RMQR	69–72

Table 7
RMQR values for weathered granite and gneissic schist.

Parameters	Description	Rating
R_{DD}	Moderate/slight degradation	6–9
R_{DSN}	Three set plus random	8
R_{DS}	0.3 m>DS>0.07 m	4
R_{DC}	Smooth	15
R_{GWSC}	Wet to dripping	3–5
R_{GWAC}	Slightly absorptive	4
	RMQR	40–45

Table 8
RMQR values for facture/shear zones in granite and gneissic schist.

Parameters	Description	Rating
R_{DD}	Moderate/slight degradation	1–3
R_{DSN}	Four set plus random/crushed	1–4
R_{DS}	0.07 m>DS	1
R_{DC}	Slicken-sided / thick fill	1–7
R_{GWSC}	Flowing/gushing	0–1
R_{GWAC}	Highly absorptive/extremely absorptive	0–2
	RMQR	4–18

6.1. Previous studies stress state of Afghanistan and its implications on tunnel sites

Aydan et al. [27] reported a detailed study on the stress state of Afghanistan. Their study considered faults striations, focal mechanism solutions, GPS measurements [3,4,11,12]. The results of this study and its implications on the stress state of the tunnel sites are summarized herein.

6.1.1. Stress inferences from fault striations or sense of deformation

The data on the striations of major faults of Afghanistan are not available except a few locations due to security reasons during the site-explorations. There are several compilations of fault data. However, the dip direction and striation angles are mostly missing. A database on the orientation and rake angle of faults is prepared and utilized and the normalized maximum and minimum horizontal stresses by the vertical stress were inferred. The results indicated that the maximum horizontal stress ratio was up to 3 times and the minimum horizontal stress ratio 0.48 in Afghanistan. The stress state in the close vicinity of the Salang Tunnel site indicated that the maximum horizontal stress ratio is less than 1.5 times, and the minimum horizontal stress ratio is greater than 0.5.

6.1.2. Stress inferences from focal mechanism of earthquakes

This method has been employed, and the focal plane solutions of earthquakes since 1976 were utilized. The utmost care was taken to select the appropriate fault plane on the bases of the tectonics and previously published fault maps. When there were too many earthquakes (e.g., Hindu-Kush Mountains and Suleiman Mountain Range) the number of events reduced by giving an emphasis to the magnitude of the event. Fig. 19 shows the contours of normalized maximum and minimum horizontal stresses by the vertical stress. The results indicated that the maximum horizontal stress ratio was up to 2.8 times and the minimum horizontal stress ratio 0.34 in Afghanistan.

6.1.3. Stress inferences from GPS measurements

From Aydan [4,5,11,12], it is geometrically possible to compute strain rate components on a plane tangential to the earth's surface from the variation of positions of stations at a given time interval. Compared to other countries, Afghanistan has only a single GPS station located in

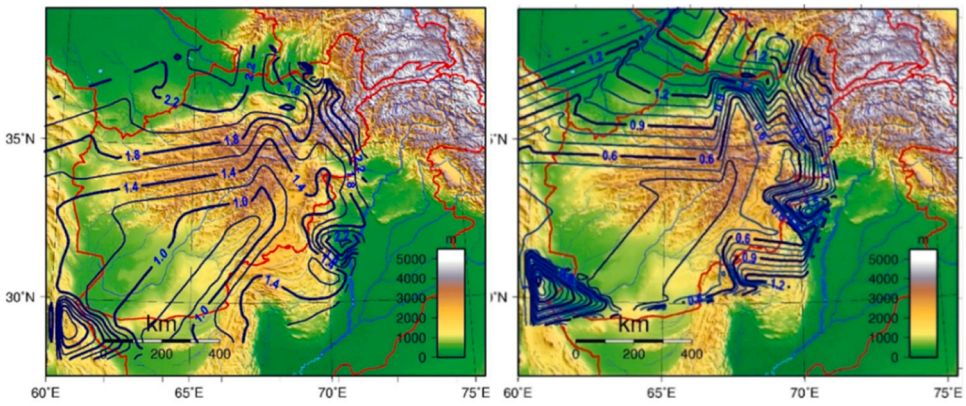

(a). Maximum horizontal stress *(b). Minimum horizontal stress*

Fig. 19. Contours of horizontal stress ratios (max and mini) normalized by vertical stress inferred from the focal mechanism solutions using Aydan's method.

Kabul. Nevertheless, the available data of GPS stations in Kabul and other GPS stations in the neighbouring countries have been utilized to evaluate the crustal deformation and straining in Afghanistan and its close vicinity and annual crustal velocity and computed principal stress variation and orientations. 20(a) shows the annual deformation rate of Afghanistan and neighboring countries while Fig. 20(b) shows the amplitude and orientation of pincipal stress rates. As the vertical component of stress tensor rates can not be obtained from GPS measurements, these principal stress rate components correspond to the maximum and minimum horizontal stress rate components. As seeen from the Figure, Afghanistan is compressed in NE-SW direction and tends to rotate clock-wise. Furthermore, stress rate components are larger in the Northern Afghanistan and Makran subduction zone as expected. Although the technique based on the GPS measurments can not yield absolute stresses, the direction of maximum horizontal stress in the close vicinity of the tunnel site can be inferred. As noted from Fig. 20(b), the maximum horizontal stress direction is NW-SE provided that the absolute and rate of stress components are co-axial.

There are some studies on the stress direction of Afghanistan utilizing the database of World-stress mapping project [35] The compiled direction of p-axis solutions of earthquakes were NS in Makran subduction zone and another subduction zone in Tajikistan. The p-axis solutions along Chaman fault and Suleiman Mountain area are NW-SE while they are NE-SW direction in the close vicinity of Sistan Sture Zone in Eastern Iran. The p-axis direction in the Hindu-Kush Mountain range typically runs northwest to southeast, indicating that the maximum horizontal stress acts perpendicular to the axis of the Hindu Kush Mountain range.

6.2. *Inference of In-situ stress state of tunnel site*

Two major earthquakes occurred approximately 100 km from the tunnel. Malistani et al. [42,40] examined the stress state in the close vicinity of Salang Tunnel, deriving the stress state using the method proposed by Aydan [13,3]. They utilized the focal mechanism solution obtained by Abers et al. [1] for the earthquake with a magnitude of 6.6 on June 24, 1972. As the direction of p-axis of the focal mechanism solutions of earthquakes in the Hindukush Mountain range is generally NW-SE, the maximum horizontal stress is likely to act perpendicular to the axis of the mountain range and parallel to the axis of the tunnel.

The predicted stress states for the earthquakes on the Andarab Fault and Hari-Rod Faults, calculated using Aydan's method [3], are illustrated in Fig. 21. For the Andarab Fault, the maximum horizontal stress aligns in the NW-SE direction, whereas for the Hari-Rod Fault, it is predominantly in the almost east-west (E-W) direction.

The solutions indicated that maximum and minimum horizontal stresses normalized by vertical stress were 1.232 and 1.093, respectively. This stress state was actually very favorable for tunnels as the

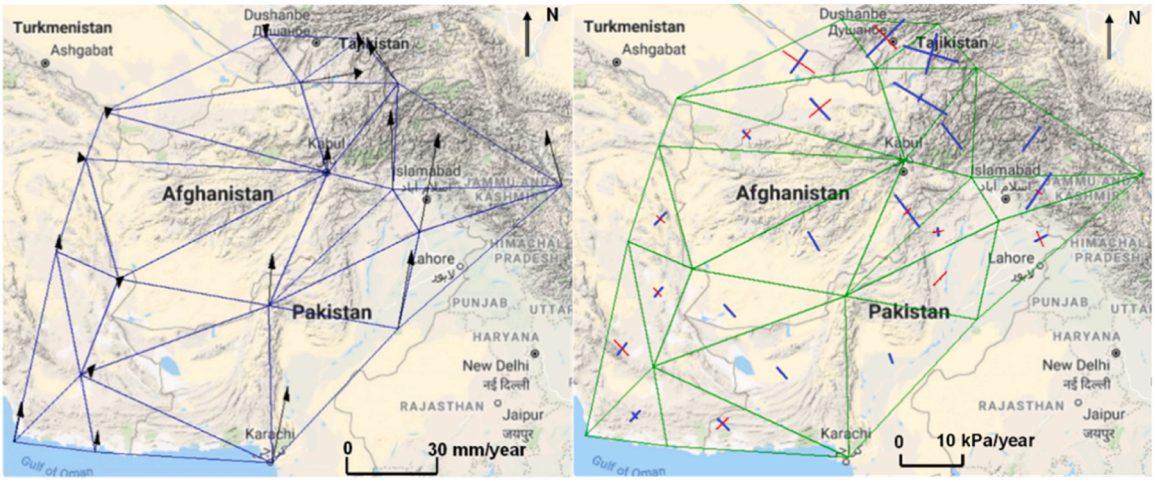

(a). Crustal annual velocity *(b). Computed principal stress rates*

Fig. 20. Crustal deformation and computed principal stress rates (from [12]).

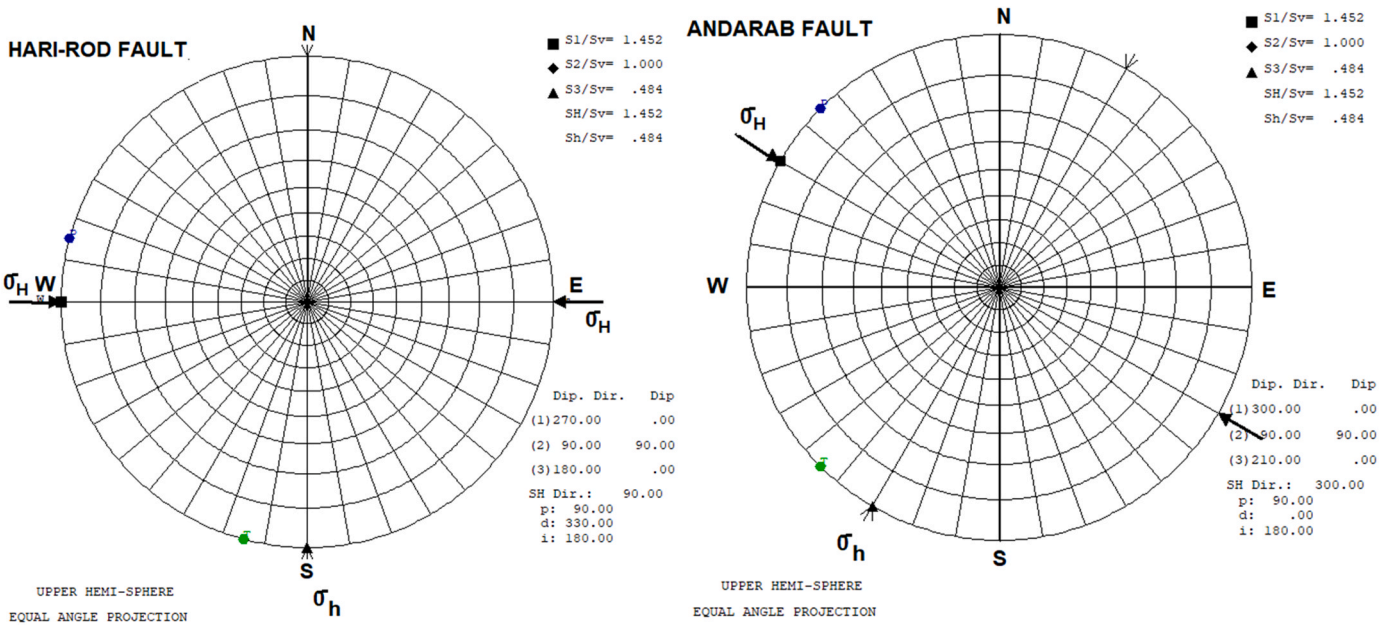

Fig. 21. Estimated in-situ stresses from Andarab and Hari-Rod faults.

stress state is close to hydrostatic in-situ stress state. However, the lateral stress acting on the tunnel cross-section is almost close to unity as estimated previously [42,40]. These inferences are also in good agreement with the quantitative estimations by Aydan et al. [27] and they definitely provide some quantitative data for the stress state of the tunnel site.

7. Estimation of rock mass propertes

Any rock engineering evaluation of the stability of underground spaces such as tunnels requires the following properties of surrounding rock.

1. Uniaxial compressive strength (UCS),
2. Uniaxial tensile strength,
3. Elastic modulus,
4. Passion's ratio,
5. Friction angle, and
6. Cohesion of intact rock.

Aydan et al. [22] introduced equations linking six essential mechanical properties of rock masses to RMQR. They proposed a unified expression that relates any rock mass's mechanical properties to those of the intact rock.

$$\alpha = \alpha_0 - \frac{(\alpha_0 - \alpha_{100})RMQR}{RMQR + \beta(100 - RMQR)} \quad (1)$$

Where $\alpha_o$and α_{100} are the values of the function at RMQR = 0 and RMQR = 100 of property α and β is a constant to be determined by using a minimization procedure for experimental values of given physical or mechanical properties. Values for these empirical constants with the consideration of in situ experiments carried out in Japan and compiled by Aydan et al. [22] are shown in Table 9. When a representative value of RMQR is determined for a specific site, the geomechanical properties of the rock mass can be derived using Eq. (1), in conjunction with the constants provided in Table 9 and the intact rock values for the desired property. The details of the application of RMQR to in-situ experimental result for the estimation of geomechanical properties of rock masses can be found in Aydan et al. [22].

Using intact properties for fresh rock according to the designation of

Table 9
Values of and for various properties of rock mass (from [22]).

Property (α)	α_o	α_{100}	β
Deformation modulus	0.0	1.0	6.0
Poisson's ratio	2.5	1.0	1.0
UCS	0.0	1.0	6.0
Tensile strength	0.0	1.0	6.0
Cohesion	0.0	1.0	6.0
Friction angle	0.3	1.0	1.0

MOPW and RMQR values for rock mass, the rock mass properties are estimated from five different values of RMQR including the fault/shear zone (RMQR=13) and relations given by Eq. (1) as given in Table 10. The characterization of fault and shear zones is based on a recent study conducted by Aydan et al. [24].

8. Stability analyses

In this section, several stability analyses will be discussed, utilizing an integrated approach introduced by Aydan [6,8].

8.1. Block stability problems

Four discontinuity sets have been identified, as depicted in Fig. 18. The projection of these discontinuity sets onto the tunnel cross-section is illustrated in Fig. 22. It is very likely that blocks bounded by

Table 10
Estimated mechanical properties rock mass.

Properties of Rock Mass	Intact Rock (fresh)	RMQR				
		40	50	60	70	Fault Zone
UCS (MPa)	100	10.0	14.3	20.0	28.0	2.5
Elastic Modulus (GPa)	50	5.0	7.14	10.0	14.0	1.25
Poisson's ratio	0.2	0.38	0.35	0.32	0.29	0.46
Cohesion (MPa)	14	1.4	2.0	2.8	3.92	0.35
Tensile Strength (MPa)	8	0.8	1.14	1.6	2.24	0.20
Friction Angle (°)	60	34.8	39.0	43.2	47.4	23.5

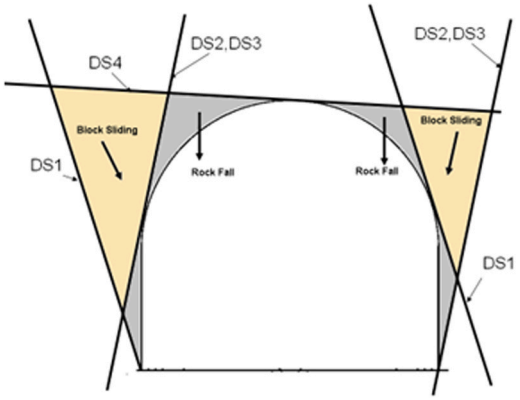

Fig. 22. Potential block stability problems around the tunnel.

discontinuity sets DS2, DS3, and DS4 would collapse into the opening immediately after excavation. Additionally, smaller blocks at the sidewalls, bounded by DS1, DS2, and DS3, might have also fallen or slid into the opening shortly after excavation. Larger blocks at both shoulders of the openings are at risk of sliding into the opening if no countermeasures are taken. Specifically, precautions are crucial during the excavation of the tunnel's west side wall. Without measures such as quick shotcreting and the installation of rockbolts, significant overbreaks, rockfalls from the roof, and sliding of blocks from the west sidewall into the tunnel may occur.

8.2. Estimation of stress induced slip/separation zones around tunnels

As discussed, four discontinuity sets have been observed in the vicinity of the tunnel. These discontinuities, which are structural defects within the rock mass, would play a significant role regarding local failures [2], which may be of great concern during excavations and computing rock loads on the support system. However, these discontinuities may also have a positive effect by reducing stress concentrations around the tunnel. The authors conducted analyses to assess the extent of yielding, including slip or separation, involving discontinuity sets, utilizing the method developed by Aydan (e.g., [8,10]). The shear resistance of the discontinuity sets is assumed to be frictional, and the friction angle was set to 35 degrees to be on the safe side in view of friction tests described, previously. Fig. 23 shows the yield zone of each discontinuity set around the tunnel, which is about 4 m from its perimeter. The recent boring data in the existing tunnel such zones do

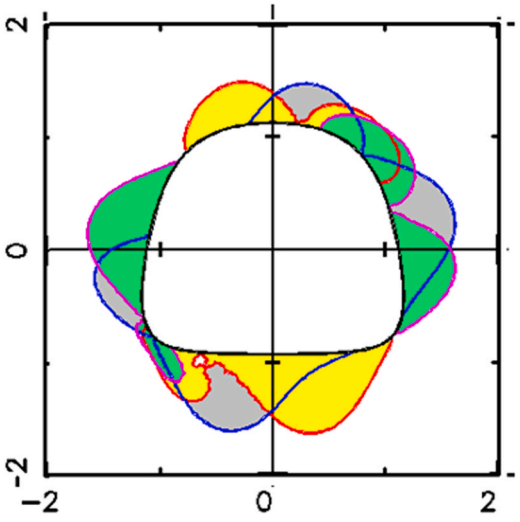

Fig. 23. Yield zones associated with discontinuity sets.

exist in surrounding rock mass. These estimations also imply that rockbolt length should be greater than 4 m in the roof and sidewalls for safety.

8.3. Ground reaction response analysis using analytical approaches

The ground reaction response approach may be related to the study of Fenner [34]. This model is based on the elastic-perfectly plastic behavior, implying the tunnel would be stable without any support. This method has been improved recently by considering different yield criteria and constitutive models (e.g. [37,18,19,20,26]).

8.3.1. Existing tunnel

Laboratory tests conducted on the mechanical properties of granite have shown a wide range of UCS (Uniaxial Compressive Strength) values. The average UCS value inferred from point-load tests conducted near outcrops and boreholes in the existing tunnel was approximately 55 MPa, as reported by MOPW. Aydan et al. [18,19,20,26] developed a technique to assess the squeezing potentials of rocks in tunneling, later extending it to evaluate rock burst potential in tunneling by Aydan et al. [26]. Rock mass properties were estimated using RMQR and various relations proposed by [18,19], and several analyses were performed. The RMQR values ranged from 40 to 60, as indicated in Tables 4 and 5. It was assumed to be uniform along the alignment of the existing tunnel due to the lack of sufficient investigation into rock mass conditions. Fig. 24 illustrates tunnel wall strain, plastic zone radius, and the level of squeezing/bursting (which implies squeezing or bursting) along the tunnel alignment concerning the overburden. The maximum overburden of the existing tunnel is approximately 400 m. The results demonstrate that stress-induced strains and plastic zones expand significantly where the overburden reaches 400 m. The computed results for three different values are likely representative values for the tunnel.

Further computations were conducted for the section with the maximum overburden. Fig. 25 displays the computed ground reaction curves for three different RMQR values. Rock mass strength was estimated using the method proposed by Aydan et al. [22], incorporating RMQR and the intrinsic properties of intact rock. The computation indicated that the inward displacements would be less than 90 mm in view of the tangential tunnel strain and diameter of the existing tunnel at the time of construction.

8.3.2. Planned tunnels

The average value of the UCS obtained from boreholes along the alignment of the planned tunnels for rock designated as "fresh" was about 100 MPa according to the reports by MOPW. The technique of Aydan et al. [18,19,26,29] together with RMQR values of 50, 60 and 70 are also used for planned tunnels to evaluate the squeezing or rockbursting levels of rocks in tunneling. Fig. 26 illustrates the tunnel wall strain, plastic zone radius, and the level of squeezing/bursting along the tunnel alignment concerning the overburden. The maximum overburden of the tunnel is about 842 m for the planned tunnels. The results for the planned tunnels indicate that stress induced strains and plastic zones become larger if the RMQR values are reduced from 70 to 50. The plastic straining and level of squeezing/rockbursting (which implies either squeezing or rockbursting) would be quite severe for the tunnels with RMQR value of 50 at the sections with high overburden.

Fig. 27 shows the ground reaction curves computed for the planned tunnels. For three RMQR values rock mass strength was estimated from the procedure proposed by Aydan et al. [22] using intrinsic properties of intact rock and other properties obtained from the relation proposed by Aydan et al. [18,19,22]. The computation indicated that the inward displacements would be less than 2 mm for RMQR=70 while it will be about 21 mm for RMQR=50. However, it should be noted that the rock mass may burst if the support pressure is less than 0.35 MPa under such conditions. In other words, the rock mass should not allow to be strained

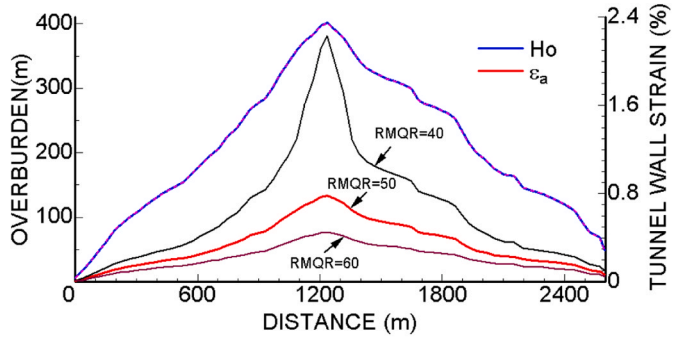

(a). Tunnel wall strain

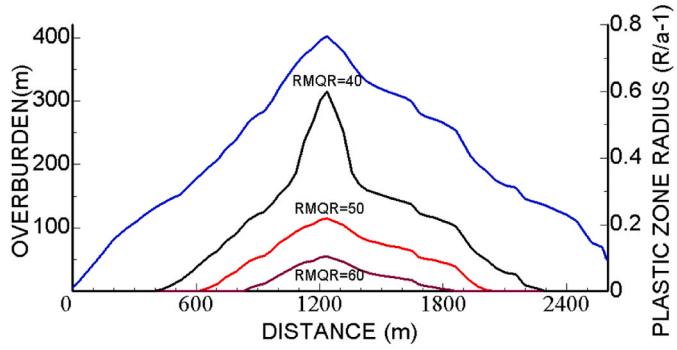

(b). Plastic zone radius

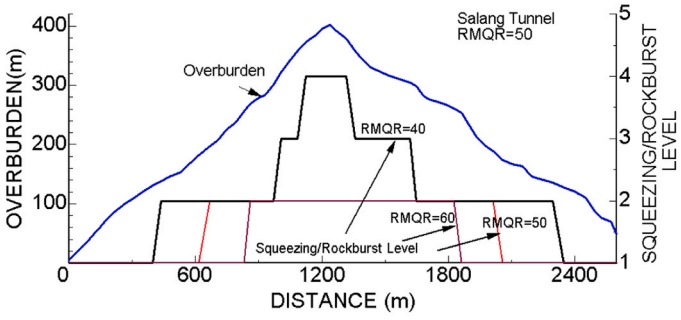

(c). Degree of squeezing and bursting

Fig. 24. The tunnel-wall strain, plastic zone radius and level of squeezing/ bursting computed values.

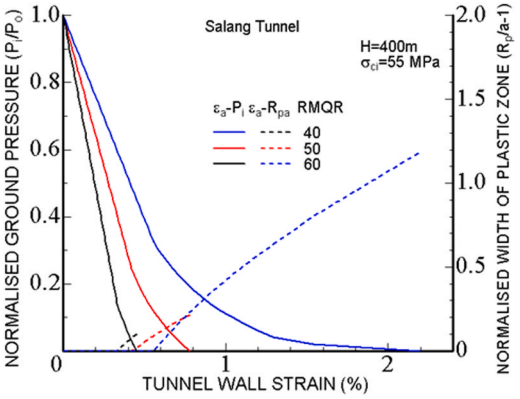

Fig. 25. Computed ground-reaction curves.

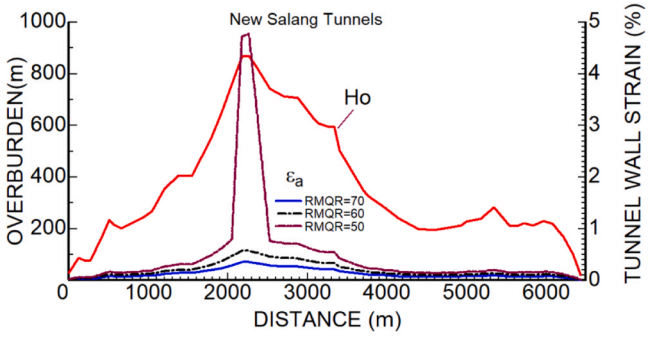

(a). Tunnel wall strain.

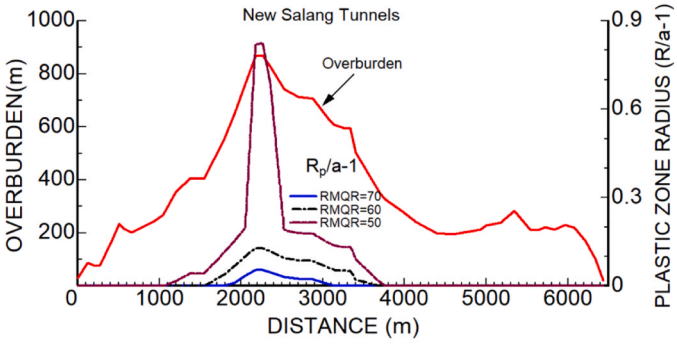

(b). Plastic zone radius

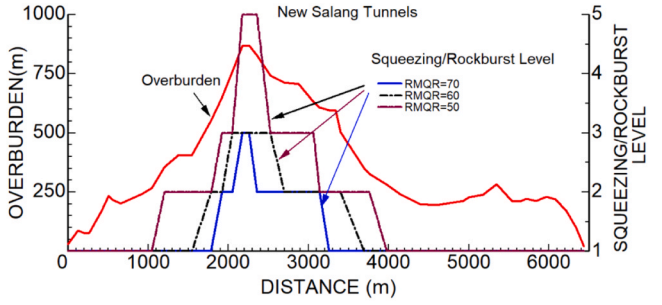

(c). Degree of squeezing/bursting

Fig. 26. Computed tunnel-wall strain, plastic zone radius and level of squeezing or bursting for south and north tunnels.

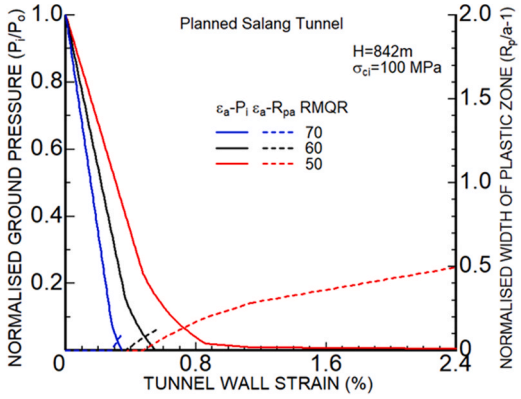

Fig. 27. Computed ground-reaction curves for the highest overburden.

more than 0.86%.

As shown in Fig. 4, the planned tunnels are anticipated to cross 5 fault zones. A preliminary analysis was carried out for the fault/shear zone with highest overburden (600 m) and estimated material properties given in Table 10 and ground-reaction curves are shown in Fig. 28. These preliminary analyses indicate that the tunnels would definitely show heavy squeezing response at fracture/shear zones. The estimated convergence may be greater than 1000 mm. There is no doubt that some proper countermeasures would be necessary against large ground deformation at such zones. For example, trimming of the tunnel after large deformations may be necessary to deal with such issues.

8.4. Elasto-plastic finite element analyses

An elasto-plastic finite element analysis was conducted to assess the stability of the existing tunnel. Fig. 29 depicts the Finite Element Method (FEM) mesh used in the analysis. The material properties utilized for the analysis are outlined in Table 11. Fig. 30 illustrates the distribution of maximum shear stress around the tunnel. The results indicated potential instability issues at the lower corners of the tunnel. Therefore, a 5-center-circular with invert cross section shape is suggested.

Several elastic finite element analyses were performed on the stability of the planned tunnels. Material properties used in the analyses are given in Table 11 for the south and north tunnels. Figs. 31 and 32 show the distributions of ground displacement and the maximum shear stress, respectively, at the locations where the overburden is highest. As noted from the maximum shear distribution around the tunnels, some instability problems may appear at the lower corners of the tunnel, particularly. As the rock mass is granite, it is very likely that severe rock burst problems may be encountered as observed in Mont Blanc Tunnel between France and Italy [44], Shimizu Tunnel in Japan [45], Gothard Tunnel [36], and Jingping Tunnel in China [38], recently (see [17,14] for details).

Although the analyses shown herein are for elastic cases, it is necessary to carry out elasto-plastic and/or elasto-visco-plastic analyses on the bases of the analytical estimates shown in Figs. 27 and 28. Furthermore, numerical analyses should be incorporating the support members such as rockbolts, shotcrete, steel ribs and concrete lining with appropriate numerical representations and constitutive laws [2,8]. In such analyses, the effectiveness and responses of support members under such high in-situ stress conditions should be truly evaluated and discussed. Therefore, a five-center circular with invert shape is suggested for the tunnel cross section.

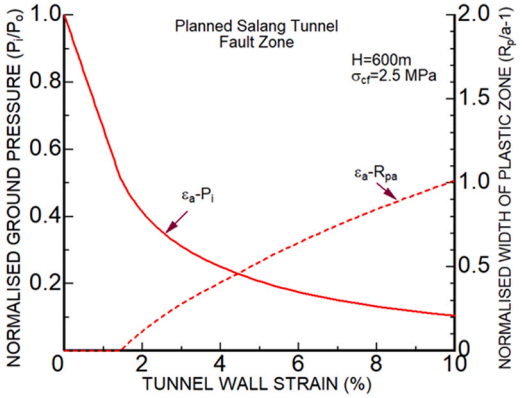

Fig. 28. Computed ground-reaction curve for fault/shear zone.

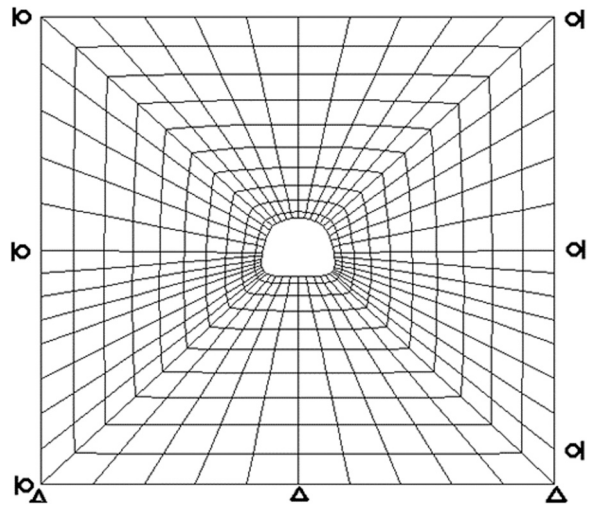

Fig. 29. Finite element mesh and boundary conditions.

Table 11
Material properties used in FEM analyses.

UW (kN/m3)	E (GPa)	ν	c (MPa)	σ_t (kPa)	φ (°)
26	1.4	0.3	2	0.6	35

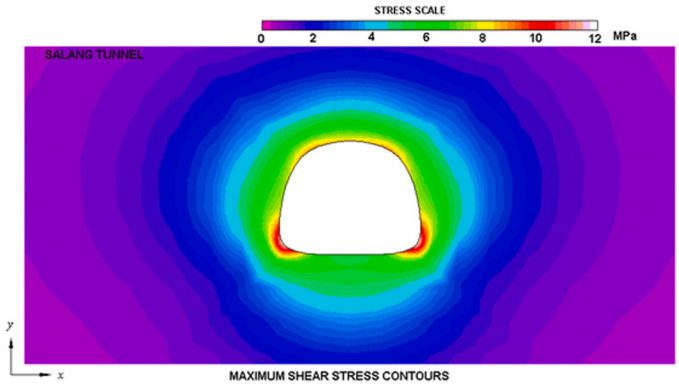

Fig. 30. Maximum shear stress contours.

9. Support design philosophy and suggested rock support systems

9.1. Integrated and unified support design philosophy

The design of underground structures is generally done utilizing empirical methods such as rock classifications and/or with the help of some theoretical methods and model tests before the computers have become available to geo-engineers. The present tendency is also to use numerical techniques such as finite element and boundary element methods for design purposes. Due to the inherent presence of numerous discontinuities in rock masses, there is no unified method for design of underground structures. Different approaches are often required to account for these complexities.

Furthermore, it is always an important issue how to assess the global and local stabilities around underground openings. Fig. 33 shows a proposal suggested by Aydan [2,6,8] for assessing the global and local stabilities around underground openings.

Aydan [2,6,8] suggested that the structural defect approach and the rock-support interaction approach can be unified for a more generalized

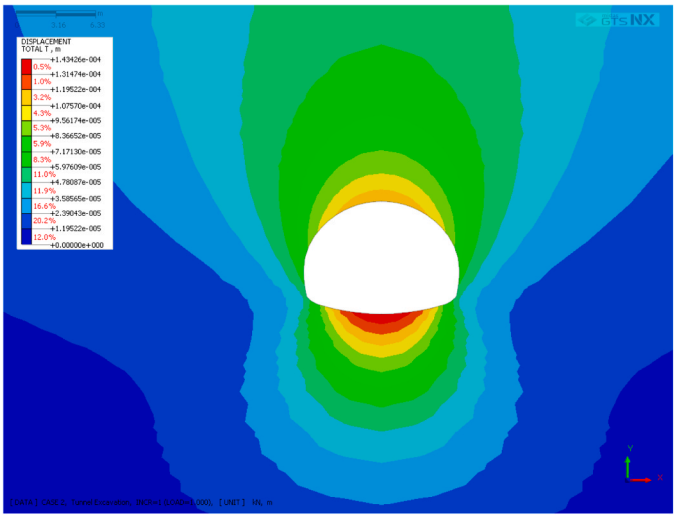

Fig. 31. Displacement contours.

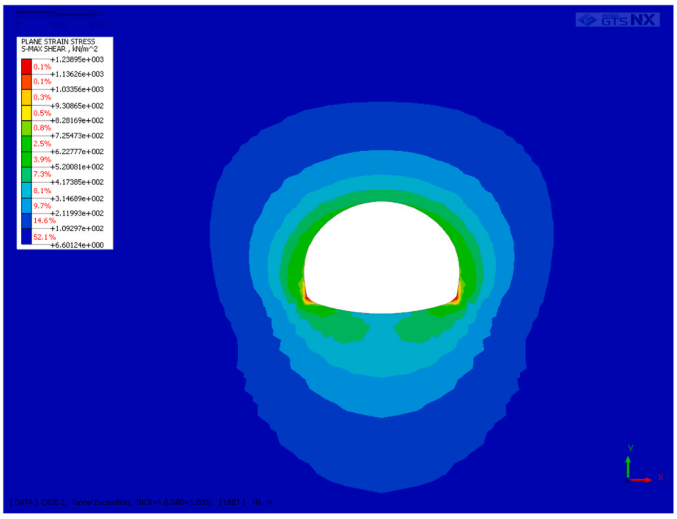

Fig. 32. Maximum shear stress contours.

approach. This unification assumes that there are four zones, namely, elastic zone, the plastic zone, the loosening zone and the zone due to structural defects, about the opening. The conditions for the appearance of such zones are

- The ***structural defect zone*** can occur when rock mass has one discontinuity set or more, and at least one of which daylights on the surface of the opening.
- The ***loosening zone*** can occur when the initial in-situ stress ratio and the geometry of the effective opening shape defined by the geometrical orientation of structural defects (discontinuity sets) are such that tensile stress regions about the opening are to occur. Note that the term of loosening zone is herein associated with the zone caused by tensile stresses, which the rock mass may not sustain and becomes free from the true ground stress field about the opening. It is distinguished from the zone created by the plastification of rock due to compressive stress field.
- The ***plastic zone*** can occur if the redistributed stress state is such that it is sufficient to cause the yielding of rock in the region outside the possible above two other zones.

All these three zones described above may not be observed in every excavation and their occurrence would depend upon the conditions such as the geologic structure of rock mass, the geometry of the opening, the initial in-situ stress field and the mechanical properties of rock. Therefore, there may be a number of varieties in real rock engineering practices. The present philosophy of underground structures design may be outlined as follows [6,8] (Fig. 34):

Stage I): Geological and geophysical investigations and testing:
Stage II) General Evaluation:
Stage III) Global and Local Stability Assessment:
Stage IV) Detailed Stability Analysis Against Global and Local Instability Modes

1. Rock masses are generally modeled by three models for both global and local instability modes:
   a-) Equivalent mass approach:
   b-) Semi-explicit continuum models:
   c-) Explicit approaches:
2. The methods of analysis of the stability of tunnels are chosen:

a-) Closed-form Methods:
b-) Numerical Methods:
c-) Limiting equilibrium approaches:
Stage V) General Assessment and Final Design:
Stage VI) Construction and Back Analyses:

In general sense, the support design involves the dimensioning of rockbolts, steel sets, shotcrete and concrete lining [2,8]. Concrete lining is frequently employed as a support structure, primarily to enhance airflow, prevent groundwater ingress into the tunnel, and serve as an additional safety measure.

9.2. Current design of tunnel support systems and rock load concept

The current design of the tunnel support system is still based on rock load concept initially proposed by Terzaghi in 1946 on the basis of his trap door experiments. The support system, which is generally concrete lining, is isolated from the surrounding rock mass and assumed to be partly supported by ground reaction springs and rock loads are imposed on the structure. Despite the use of very sophisticated numerical analyses, the design is still based on this very primitive concept. Following Terzaghi's proposal, the rock load concept, which is fundamentally corresponds to dead-weight of certain region of loosened rock in the roof and sidewalls, is also used by many modern rock mass classifications (e.g., Q-System, RMR etc.) for the design of underground structures. The major issue is how to determine such loads. The modern rock mass classifications just assume that a certain height of the loosening zone as a function of rock mass classification number (e.g., RQD (Deere), Q-System (Barton) [31] RMR [32,33] etc.). Table 12 shows rock loads coefficients (h/B) suggested by various rock mass classifications.

These rock load concepts have been explained through some arching theories proposed by Terzaghi [47] and Protodyakonov (see [46]). Terzaghi's Arching Theory is developed by assuming yielding along vertical plane.

$$\frac{h}{B}=\frac{1}{2K_0\tan\varnothing} \tag{2}$$

Where h,B,$K_o$and $\varphi$are load height, tunnel width, horizontal pressure coefficient and friction angle. On the other hand, Protodyakonov's arching theory is based on the yielding along horizontal planes and the following formula is obtained.

$$\frac{h}{B}=\frac{1}{2\tan\varnothing} \tag{3}$$

As the value of the lateral pressure coefficient is almost equal to 1, both formulae take the same form. For very loose fractured or granulated ground, the friction angle is about 30 degrees. For this situation, the rock load coefficient would be about 0.87.

If the plastic zone is formed as a result of brittle behavior without any cohesive strength, the gravitational effect in plastic zone is included in

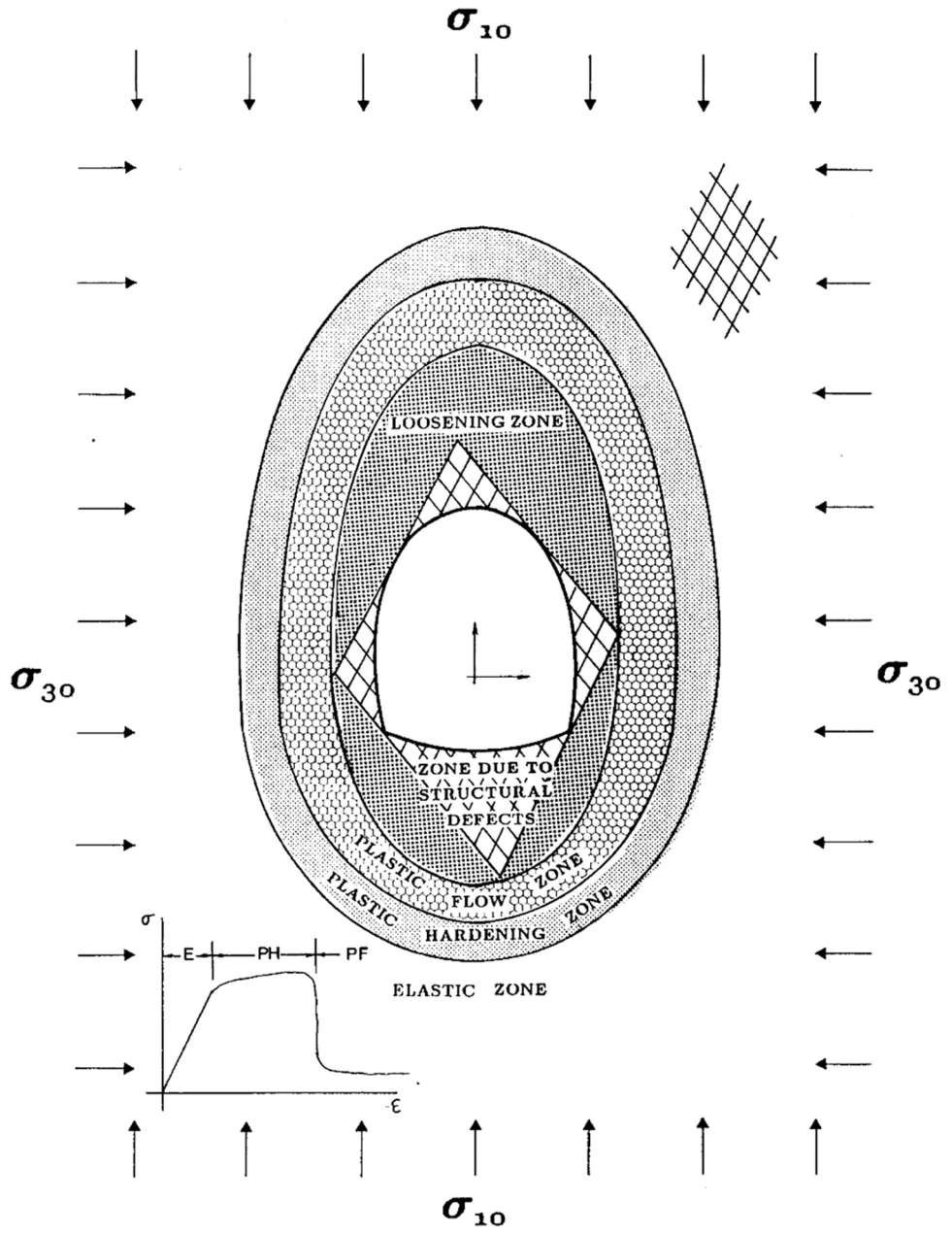

Fig. 33. An illustration of plastic zones, the loosening zone, and the zone due to structural defects (from Aydan [2,6,8]).

the formulation of ground-reaction approach. The rock load under such condition can be given by the following formula (e.g., [2])

$$\frac{h}{B}=\left[1-\left(\frac{a}{R_p}\right)^{q^*-2}\right]\frac{1}{2}\frac{1}{q^*-2} \tag{4}$$

where

$q^*=\frac{1+\sin\varphi^*}{1-\sin\varphi^*}$; φ^* friction angle of plastic zone.

For very large values of plastic radius, this formula will converge to

$$\frac{h}{B}=\frac{1}{2}\frac{1}{q^*-2} \tag{5}$$

Similarly for friction angle of 30 degrees, the rock load coefficient will have the value of 0.5. It should be also noted that if rock mass behaves in perfectly plastic or strain hardening manner, the effect of gravity should be almost negligible despite some take into account such effects without any consideration of constitutive law assumed in formulations. It should be also noted that the rock-load under seismic conditions would be increased during and following earthquakes as experimentally shown by Aydan [8]. In addition to rock loads described above, the rock loads resulting from structural defects can be obtained using the procedures described by Aydan [2,8].

The numerical methods are often utilized to check the response of support members. For low overburden, the support system may behave elastically for an overburden height of 200 m. However, the supports system consisting of rockbolts and shotcrete may yield under high overburden pressure [25,2,8]. Particularly, the rockbolts with platens may be thrown into the excavation space like a bullet, if they are not extendable or deformable. Despite these issues, the present numerical analyses often ignore this aspect. In other words, the utilization of such numerical analyses should not be allowed and accepted unless all computed data are presented and truly discussed.

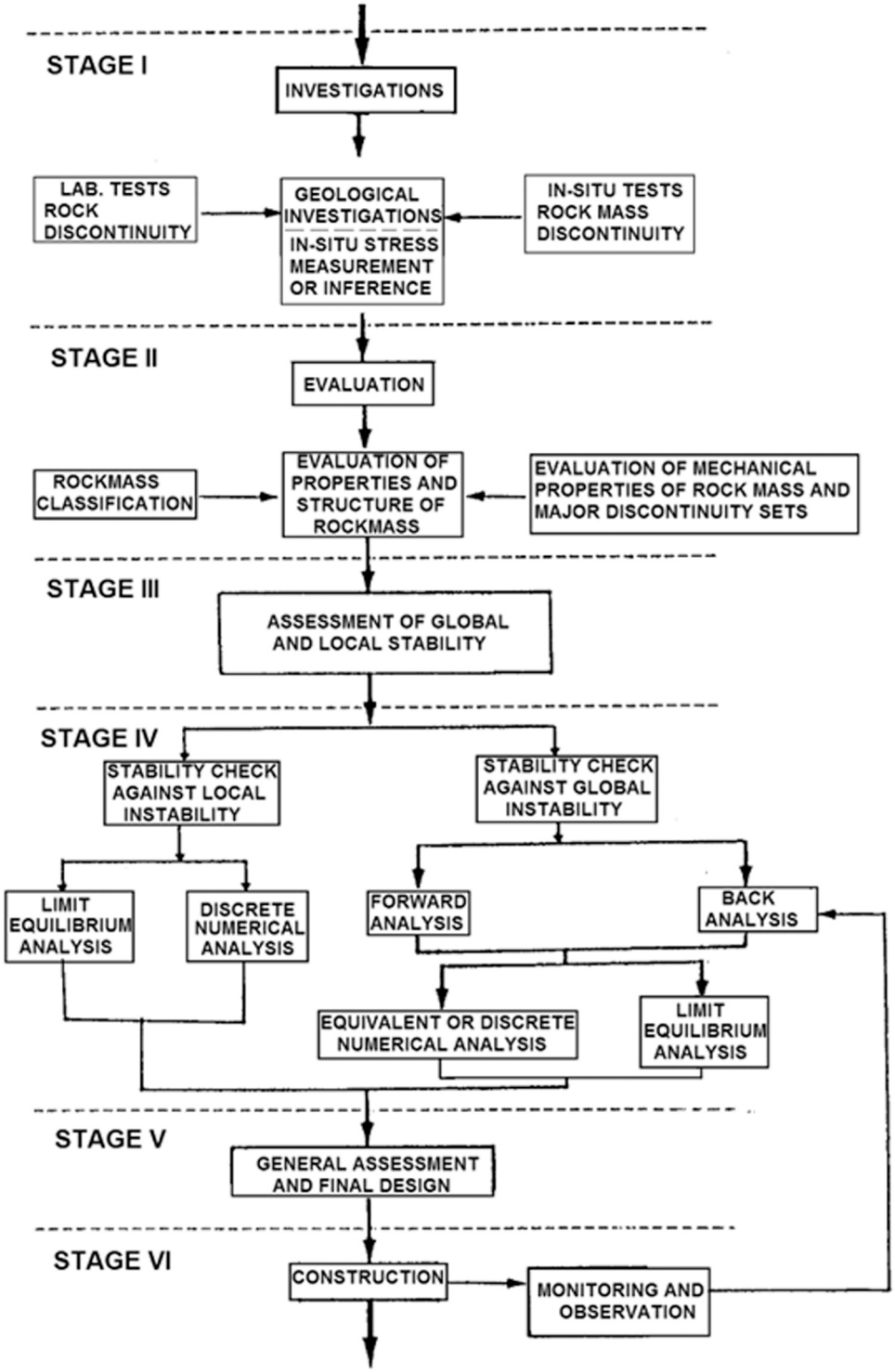

Fig. 34. Flow chart of design and construction of an underground structure [6,8].

9.3. Empirical tunnel support systems based RMQR

Aydan and Ulusay [16] established some empirical guidelines for the design of support systems based on the RMQR rock classification system as given Table 13. This proposal would be appropriate for tunnels, which are not subjected to heavy squeezing or bursting conditions. If squeezing or bursting conditions are of great concern, the appropriateness of the support system must be analyzed in detail with appropriate numerical representations and constitutive modelling of the support members.

In addition to rock mass classifications according to RMQR, some correlations with rock mass classification systems used in Japan have been explored and the results are given in Table 13 for the existing Salang Tunnel. As mentioned earlier, the rock masses near the portals are typically fractured and altered. Consequently, it is expected that the actual rock mass conditions will improve as one moves away from the portals, excluding fault and fracture zones.

In the existing tunnel, Table 15 outlines specific values for the support system. As indicated in the table, the Q-System implies a very light support system in comparison to the RMQR and NEXCO methods. The RMQR rock classification suggests a slightly more conservative support

Table 12
Rock load coefficients (h/B) among various rock classifications (from [2]).

TERZAGHI		DEERE			BIENIAWSKI		BARTON	
Class	Rock Load	Class	Rock Load		Class	Rock Load	Class	Rock Load
1	0	1	TBM	0.0-0.2	1	0.0-0.2	1	0
			DB	0.0-0.3			2	0.0-0.08
3	0.0-0.25		TBM	0.0-0.4			3	0.08-0.12
2	0.0-0.50	2	DB	0.3-0.6	2	0.2-0.4	4	0.12-0.36
4	0.25-2.2	3	TBM	0.4-1.0	3	0.4-0.6	5	0.36-0.50
			DB	0.6-1.3			6	0.50-0.77
5	0.70-2.2	4	TBM	1.0-1.6	4	0.6-0.8	7	0.77-1.66
			DB	1.3-2.0				
6	2.2	5	TBM	1.6-2.2	5	0.8<	8	1.66-3.57
			DB	2.0-2.8				
7	2.2-4.2	6	upto 75 m					
8	4.2-9.						9	3.57-7.7
9	upto 75 m							

Table 13
Support systems for tunnels (D or B, 10 m span) *.

RMQR range	Rockbolts		Shotcrete	Steel ribs		Wire mesh	Concrete Lining (mm)	Invert	
	L_b (m)	e_b (m)	t_s (mm)	Type	e_r (m)			Lining (mm)	Bolt L (m)
100≥RMQR>95	-	-	-	-	-	-	-	-	-
95≥RMQR>80	2–3	2.5	50	-	-	-	-	-	-
80≥ RMQR>60	3–4	2.0	100	Light	1.5	Yes	200	-	-
60≥ RMQR>40	4–5	1.5	150	Medium	1.2	Yes	300	300	-
40≥ RMQR>20	5–6	1.0	200	Heavy	1.0	Yes	500	500	5–6
20>RMQR	6–7	0.5	250	Very heavy	0.8	Yes	800	800	6–7

L: length; e: spacing; t: thickness; Bolt: 200 kN; Anchor; 400 kN; UCS of shotcrete: 10 MPa; S: Span (width); H: Height).
*When RMQR<30, UCS of intact rock is less than 20 MPa and overburden is greater than 100 m, squeezing problems may be encountered. Under such circumstances, forepoles, face bolting and shotcreting may be required.

Table 14
Rock classes of the existing and planned Salang Tunnels according to various rock mass classifications systems.

Classification	Rock Class
RMQR	IV (Fair to Medium)
DENKEN	CM
NEXCO	CII
JR	III_N-II_N
Q-System	Poor

Table 15
Support system design according to the classifications for the existing tunnel.

Support Member	RMQR	Q-System	NEXCO
Shotcrete	150	40	100
Rockbolt	L=4–5 m	L=3 m	L=3 m
	1.5×1.5 m	2×2	1.5×1.5
Steel ribs	Light(H125), 1.5 m	-	H125, 1.2 m
Lining	300 mm	-	300 mm
Invert	300 mm	-	400 mm

system. However, the calculations presented in the preceding sections indicate that surrounding rock mass yielding is likely to occur when the overburden exceeds 150 m. In such cases, a support system similar to the one suggested by RMQR might be necessary. Notably, rockbolts and shotcrete were not utilized in the excavation of the existing Salang Tunnel; instead, a 650 mm thick concrete lining was constructed as a permanent support system. Furthermore, the suitability of these support systems should be evaluated through numerical analyses, as done by Malistani [39].

Based on rock mass evaluations given in Tables 5 to 7, the proposals for the design support systems given in Table 13 have also been applied

Table 16
Support system design according to the classifications for planned tunnels.

Support Member	RMQR	Q-System	NEXCO
Shotcrete	150	50–90	100
Rockbolt	L=4–5 m	L=3 m	L=3 m
	(1.5×1.5 m)	(1.7–2.5 m)	(1.5×1.5)
Steel ribs	Medium,1.2 m	-	H125,1.2 m
Lining	300 mm	-	300 mm
Invert	300 mm	-	400 mm

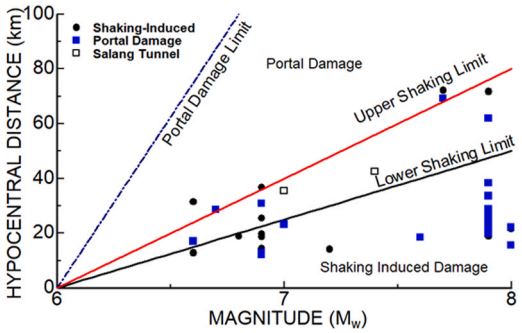

Fig. 35. Assessment of damage possibility to Salang Tunnel by earthquakes.

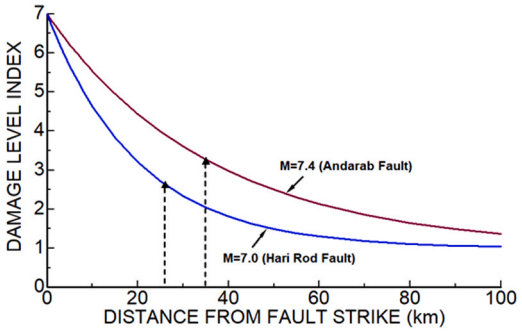

Fig. 36. Estimated DLI at Salang Tunnel for hypothetical earthquakes with a moment magnitude of 7.0 and 7.4.

to the planned Salang Tunnels and results are given in Table 16. As noted from Table 16, the Q-System suggests a very light support system compared to the RMQR and NEXCO methods. The RMQR rock classification suggests a relatively conservative support system. However, the calculations provided in the preceding subsections indicate that yielding of the surrounding rock mass is likely when the overburden exceeds 210 m. This situation might necessitate a detailed analysis of the support system recommended by RMQR, considering both overburden and rock mass conditions.

10. Consideration on the effect of nearby earthquakes on tunnels

Aydan et al. [30] compiled case histories of tunnels affected by earthquakes and proposed empirical relations for evaluating the likelihood of tunnel damage. These relations suggest that shaking-induced damage would be minimal to slight, while the portals may experience some damage during an earthquake, as shown in Fig. 35. Aydan et al. [30] also introduced a more detailed Damage Level Index (DLI). Fig. 36 illustrates the relationship between the distance from the fault strike (Rf) and the Damage Level Index (DLI). According to the figure, some damage is possible due to earthquakes on the Andarab fault and Hari-Rod fault, with the damage level index ranging between 2 and 3. A DLI of 3 might result in visible cracking of concrete lining, shotcrete, noticeable plastic deformation of rockbolt platens and steel ribs, and slight invert heaving. Conversely, a DLI of 2 may lead to hairline cracking of concrete lining and shotcrete, imperceptible deformation of rockbolt platens and steel ribs, and no invert heaving.

11. Conclusions and recommendations

This study likely represents the first geo-engineering evaluation of the existing and planned Salang Tunnels. The investigations, evaluations, and analyses offer essential insights into the probable conditions that might be encountered in both the existing and planned tunnels at the Salang Pass.

Computations indicated that stability problems such as squeezing, or rock burst could be observed during the excavation. The current evaluations provide vital information on the planned tunnels based on the sound principles of geomechanics and geoengineering. Nonetheless, the in-situ tests and investigations for the planned tunnels are still insufficient. Better evaluations could be achieved with more comprehensive investigations and experiments in the future.

The crustal stresses inferred from faults with known characteristics and focal plane solutions of Afghanistan using a method proposed by [3, 4] have been utilized to infer the in-situ stress state in the vicinity of the tunnel sites. The inferred stress states are consistent with each other, and they show similar trends. The in-situ stress conditions are expected to be close to hydrostatic stress conditions.

The support system has been assessed using different rock mass classifications including the RMQR, Q-System, and NEXCO. While the Q-system suggests a light support system, it might not be suitable in regions with significant overburden and seismic activity. Although the RMQR offers the most conservative support system, it is expected to be highly appropriate considering long-term performance, seismicity, and the potential yielding of the rock mass. However, it is important to note that specific site evaluations and analyses might be required in locations where substantial squeezing or rock burst phenomena could occur.

Groundwater and seepage pose significant challenges in the Salang Tunnel. Monitoring groundwater conditions and measuring the permeability of the rock mass, especially in fracture zones, are imperative. These measurements are invaluable for designing and implementing an efficient drainage system for the tunnel. A comprehensive understanding of groundwater behavior and rock permeability is essential for ensuring the tunnel's stability and long-term functionality. Due to the region's weather conditions and water freezing during winter, the water runoff, and its prevention from flowing onto the tunnel pavement must be managed.

Declaration of Competing Interest

The authors declare that they have no known competing financial interests or personal relationships that could have appeared to influence the work reported in this paper.

Acknowledgement

The first author was employed by the Ministry of Public Works (MOPW) of Afghanistan as a tunnel specialist associated with the rehabilitation of the existing tunnel and planning of new tunnels. The technical data utilized in this study come directly from this project, for which the authors greatly acknowledge the MOPW.

References

[1] G. Abers, C. Bryan, S. Roecker, R. McCaffrey, Thrusting of the Hindu Kush over the Southeastern Tadjik Basin, Afghanistan: evidence from two large earthquakes, Tectonics 7 (1) (1988) 41–56.
[2] Aydan, Ö. (1989). The stabilisation of rock engineering structures by rockbolts. Doctorate Thesis, Nagoya University, 204p.
[3] Ö. Aydan, A stress inference method based on structural geological features for the full-stress components in the earth' crust, Yerbilimleri 22 (2000) 223–236.
[4] Ö. Aydan, A stress inference method based on GPS measurements for the directions and rate of stresses in the earth' crust and their variation with time, Yerbilimleri 22 (2000) 21–32.
[5] Aydan, Ö. (2013): Inference of Contemporary Crustal Stresses from Recent Large Earthquakes and Its Comparison with Other Direct and Indirect Methods. 6th International Symposium on In Situ Rock Stress (RS2013), Sendai, Paper No. 1051, 420-427.
[6] Ö. Aydan, The state of art on large cavern design for underground powerhouses and long-term issues. The second Volume of Encyclopedia on Renewable Energy, John, Wiley and Sons, Chapter 45, 2016, pp. 465–487.
[7] Aydan, Ö. (2017): Infrared Thermographic Imaging in Geoengineering and Geoscience. Encyclopedia of Sustainability Science and Technology., ISBN 978-1-4939-2493-6, 413-438.

[8] Ö. Aydan, Rock Reinforcement and Rock Support, CRC Press, Taylor and Francis Group, 2018, p. 486.
[9] Aydan, Ö. (2019). Dynamic shear tests on rock discontinuities and some considerations. Proceedings of ISRM 14th International Congress of Rock Mechanics – Foz do Iguassu, Brazil, 957-964.
[10] Ö. Aydan, Rock Mechanics and Rock Engineering: Applications, CRC Press, Taylor and Francis Group, 2020, p. 410.
[11] Ö. Aydan, Rock Mechanics and Rock Engineering: Fundamentals, CRC Press, Taylor and Francis Group, 2020, p. 406.
[12] Ö. Aydan, Earthquake Science and Engineering, CRC Press, Taylor and Francis Group, 2023, p. 499.
[13] Ö. Aydan, Y. Kim, The inference of crustal stresses and possible earthquake faulting mechanism in Shizuoka Prefecture from the striations of faults, J. School Mar Sci. Technol., Tokai Univ. (No.54) (2002) 21–35.
[14] Ö. Aydan, M. Geniş, Rockburst phenomena in underground openings and evaluation of its counter measures, J. Rock Mech., TNGRM, Special Issue (No.17) (2010) 1–62.
[15] Ö. Aydan, R. Meyers, Ground motions and deformations associated with earthquake faulting and their effects on the safety of engineering structures, Springer, 2012, pp. 3233–3253.
[16] Aydan, Ö., Ulusay, R. (2014): Rock Mass Quality Rating (RMQR) System: Its Application to Estimation of Geomechanical Characteristics of Rock Masses and to Rock Support Selection for Underground Caverns and Tunnels. Proc. of the 8th Asian Rock Mechanics Symposium, Sapporo, 2075-2084.
[17] Ö. Aydan, Xia-Ting Feng, Subchapter 8.4: multi-parameter and infrared monitoring systems for real-time rockburst susceptibility evaluation and their applications to practice in Japan. Sub-Chapter 8.4. Rockburst: Mechanisms, Monitoring, Elsevier, 2018, pp. 282–299.
[18] Ö. Aydan, T. Akagi, T. Kawamoto, Squeezing potential of rocks around tunnels; theory and prediction, Rock Mech. and Rock Eng. 26 (2) (1993) 137–163.
[19] Ö. Aydan, T. Akagi, T. Kawamoto, The squeezing potential of rock around tunnels: theory and prediction with examples taken from Japan, Rock Mech. and Rock Eng. 29 (3) (1996) 125–143.
[20] Ö. Aydan, S. Dalgıç, T. Kawamoto, Prediction of squeezing potential of rocks in tunnelling through a combination of an analytical method and rock mass classifications, Italian Geotech. J. 34 (1) (2000) 41–45.
[21] Aydan, Ö., Tokashiki, N. and Geniş, M. (2012): Some Considerations on Yield (Failure) Criteria in Rock Mechanics ARMA 12-640, 46th US Rock Mechanics / Geomechanics Symposium, Chicago, Paper No. 640, 10 pages (on CD).
[22] Ö. Aydan, R. Ulusay, N. Tokashiki, A new rock mass quality rating system: Rock Mass Quality Rating (RMQR) and its application to the estimation of geomechanical characteristics of rock masses, Rock Mech. Rock Eng. 47 (2014) 1255–1276.
[23] Aydan, Ö., N. Malistani, N. Tokashiki (2017). The possibility of infrared camera thermography for assessing the real-time stability of tunnels against rockburst. The 51st US Rock Mechanics / Geomechanics Symposium, ARMA 17-0479, 6p.
[24] Aydan, Ö., H. Kumsar, N. Iwata (2022b). Characterization and Properties of Faults Zones and Their Effect on Stress Changes during Earthquake. RocDyn4, Xuzhou, 117-122.
[25] Aydan, Ö., Y. Ichikawa, and T. Kawamoto (1985). Load bearing capacity and stress distributions in/along rockbolts with inelastic behaviour of interfaces. Proc. of the 5th Int. Conf. on Num. Meths. in Geomechanics, Nagoya, 2:1281–1292.
[26] Ö. Aydan, M. Geniş, T. Akagi, T. Kawamoto, Assessment of susceptibility of rockbursting in tunnelling in hard rocks, Int. Symp. on Modern Tunnel. Sci. Technol., IS-KYOTO 2001 (2001) 391–396.
[27] Ö. Aydan, N. Malistani, N.Z. Nasiry, A.B. Jahed, An Integrated Study on the Stress State of Afghanistan, Eng. Geol. Geotech. Symp., ENGGEO 2021 (2022) 183–189.
[28] Ö. Aydan, N. Iwata, R. Kiyota, N. Malistani, Tilting and Stick–Slip Tests for Evaluating Static and Dynamic Frictional Properties of Rock Discontinuities, Rock Mech. Rock Eng. 56 (2023) 8607–8622.
[29] Ö. Aydan, M. Daido, H. Tano, N. Tokashiki, K. Ohkubo, A real-time multi-parameter monitoring system for assessing the stability of tunnels during excavation, ITA Conf., Istanbul (2005) 1253–1259.
[30] Ö. Aydan, Y. Ohta, M. Geniş, N. Tokashiki, K. Ohkubo, Response and stability of underground structures in rock mass during earthquakes, Rock Mech. Rock Eng. Vol.43 (No.6) (2010) 857–875.
[31] N. Barton, R. Lien, I. Lunde, Engineering classification of rock masses for the design of tunnel support, Rock Mech 6 (4) (1974) 189–239.
[32] Z.T. Bieniawski, Engineering classification of jointed rock masses, STrans. S. Afr. Int. Civ. Eng. 15 (1973) 335–344.
[33] Z.T. Bieniawski, Estimating the strength of rock materials, J. S. Afr. Inst. Min. Metall. 74 (1974) 312–320.
[34] R. Fenner, Researches on the notion of ground stress (in German), Glückauf 74 (1938) 681–695.
[35] Heidbach, O., M. Rajabi, K. Reiter, M. Ziegler, and the WSM Team (2016). World Stress Map Database Release 2016, GFZ Data Services,
[36] A. Henke, Tunnelling in Switzerland: from long tradition to the longest tunnel in the world, World Long Tunnels (2005) 57–70.
[37] E. Hoek, E.T. Brown, Underground Excavations in Rock, Inst. Min. & Metall, London, 1980.
[38] Q. Jiang, G.S. Su, X.T. Feng, J. Cui, P.Z. Pan, J.Q. Jiang, Observation of rock fragment ejection in post-failure response, Int. J. Rock Mech. Min. Sci. 74 (2015) 30–37.
[39] Malistani. N., 2017. A Fundamental Study on Integrated Tunnel Design System in Rock Masses with a Special Emphasis on Salang Tunnels, Afghanistan. Master Thesis, University of the Ryukyus, Engineering Faculty.
[40] Malistani, N., Aydan, Ö. 2016b., Preliminary Rock Engineering Assessment of New Planned Salang Tunnels, Afghanistan. 9th Asian Rock Mechanics Symposium (ARMS9), 18th to 20th Oct, Bali, Indonesia. ARMS9, Paper126.
[41] N. Malistani, M.N. Nejabi, Key Technical Considerations on Rehabilitation of Existing Salang Tunnel – Afghanistan, Taylor and Francis, London, 2019, pp. 383–388.
[42] N. Malistani, Ö. Aydan, J. Tomiyama. Preliminary Rock Engineering Assessment of Salang Tunnel, CRC Press, Cappadocia, Turkey, 2016, 763-367.
[43] Ministry of Public Works of Afghanistan (MOPW), Reports on the design and geotechnical investigations of the existing and planned tunnels.
[44] M. Panet, Quelques problèmes de mécanique des roches posés par le tunnel du Mont Blanc. Bul. Liaison Labo. Routiers P. et Ch. (N. 42) (1969) 115–145.
[45] M. Shimokawa, S. Oda, T. Kizawa, An investigation from rock-burst phenomenon in Dai-Shimizu Tunnel (in Japanese), 5th Domestic Rock Mech. Conf. 5 (1977) 79–84.
[46] K. Széchy, The Art of Tunnelling, Akadémia Kiads, Budapest, 1973.
[47] K. Terzaghi, Rock Tunnelling with Steel Supports, Commercial Shearing and Stamping Co, Youngstown, Ohio, 1946.
[48] United States Geological Survey (USGS) (2015). Earthquake database. http://earthquake.usgs.gov/earthquakes/.

Neamatullah Malistani is an Assistant Professor at Kabul Polytechnic University, Afghanistan, concurrently pursuing his Ph.D. studies at the University of the Ryukyus, Okinawa, Japan. He obtained his B.Sc. degree in Transportation Engineering from Kabul Polytechnic University in 2012, and his M. Sc. degree in Civil Engineering from the University of the Ryukyus in 2017. With experience spanning various tunnel construction projects, he has contributed significantly to both design and management aspects. His research interests encompass Rock Mechanics and Rock Engineering, Tunneling, and Underground Space Excavation.

Prof. Dr. Ömer Aydan graduated in Mining Engineering from the İstanbul Technical University, earned his master's degree from the University of Newcastle upon Tyne, and received his Ph.D. from Nagoya University, worked at Nagoya University, Tokai University and retired from the University of the Ryukyus. He has been specialized in Rock Mechanics and Rock Engineering and also Earthquake Engineering. He has published 8 books, and he is also co-author of several books. He has more than 800 published papers in his field of specialization.